JACS
JOURNAL OF THE AMERICAN CHEMICAL SOCIETY
Article
pubs.acs.org/JACS

Synthesis, Spectroscopic Properties, and Photoconductivity of Black Absorbers Consisting of Pt(Bipyridine)(Dithiolate) Charge Transfer Complexes in the Presence and Absence of Nitrofluorenone Acceptors

Charles Browning,[†,∥] Joshua M. Hudson,[†,∥] Eric W. Reinheimer,[‡,∥] Fang-Ling Kuo,[†] Roy N. McDougald, Jr.,[†] Hassan Rabaâ,[§] Hongjun Pan,[†] John Bacsa,[‡] Xiaoping Wang,[⊥] Kim R. Dunbar,*[,‡] Nigel D. Shepherd,*[,†] and Mohammad A. Omary*[,†]

[†]Departments of Chemistry and Materials Science and Engineering, University of North Texas, Denton, Texas 76203-5070, United States

[‡]Department of Chemistry, Texas A&M University, College Station, Texas 77842-3012, United States

[§]Department of Chemistry, ESCTM, Ibn Tofail University, Kenitra 14000, Morocco

[⊥]Chemical and Engineering Materials Division, Oak Ridge National Laboratory, Oak Ridge, Tennessee 37831-6475, United States

Supporting Information

ABSTRACT: The diimine−dithiolato ambipolar complexes Pt(dbbpy)(tdt) and Pt(dmecb)(bdt) (dbbpy = 4,4′-di-*tert*-butyl-2,2′-bipyridine; tdt^{2-} = 3,4-toluenedithiolate; dmecb = 4,4′-dimethoxyester-2,2′-bipyridine; bdt^{2-} = benzene-1,2-dithiolate) are prepared herein. Pt(dmecb)(bdt) exhibits photoconductivity that remains constant (photocurrent density of 1.6 mA/cm^2 from a 20 nm thin film) *across the entire visible region of the solar spectrum* in a Schottky diode device structure. Pt(dbbpy)(tdt) acts as donor when combined with the strong nitrofluorenone acceptors 2,7-dinitro-9-fluorenone (DNF), 2,4,7-trinitro-9-fluorenone (TRNF), or 2,4,5,7-tetranitro-9-fluorenone (TENF). Supramolecular charge transfer stacks form and exhibit various donor−acceptor stacking patterns. The crystalline solids are "black absorbers" that exhibit continuous absorptions spanning the entire visible region and significant ultraviolet and near-infrared wavelengths, the latter including long wavelengths that the donor or acceptor molecules alone do not absorb. Absorption spectra reveal the persistence of donor−acceptor interactions in solution, as characterized by low-energy donor/acceptor charge transfer (DACT) bands. Crystal structures show closely packed stacks with distances that underscore intermolecular DACT. ^{1}H NMR provides further evidence of DACT, as manifested by upfield shifts of aromatic protons in the binary adducts versus their free components, whereas 2D nuclear Overhauser effect spectroscopy (NOESY) spectra suggest coupling between dithiolate donor protons with nitrofluorenone acceptor protons, in correlation with the solid-state stacking. The NMR spectra also show significant peak broadening, indicating some paramagnetism verified by magnetic susceptibility data. Solid-state absorption spectra reveal further red shifts and increased relative intensities of DACT bands for the solid adducts vs solution, suggesting cooperativity of the DACT phenomenon in the solid state, as further substantiated by ν_{C-O} and ν_{N-O} IR bands and solid-state tight-binding computational analysis.

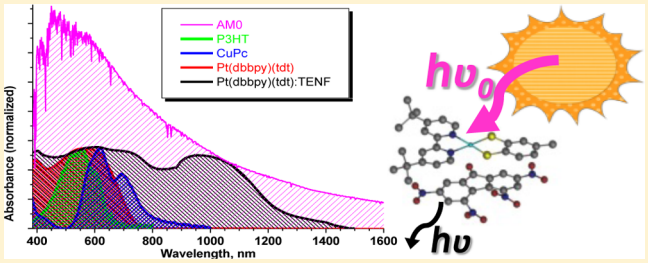

INTRODUCTION

An active area of research for over three decades has been the study of charge transfer complexes.[1−6] Thus far, several purely organic complexes have shown interesting electronic and charge transfer properties.[1] The focus of this paper, congruent with the goals of materials chemists, has been to prepare hybrid organic−inorganic materials with d−π interactions that serve to enhance those properties.[2−6] One especially fascinating result in this vein has been the preparation of a family of charge-transfer materials based on complexes such as $[Ni(dmit)_2]^{2-}$ (dmit = 2-thioxo-1,3-dithiole-4,5-dithiolate), which undergoes partial oxidation to form superconducting salts with open- and closed-shell organic cations.[2] Intermolecular interactions govern the conducting nature of these materials, with the most significant contribution to these interactions being those between the diffuse π-orbital on sulfur and the metal d-orbitals.[3] Additionally, depending on the stacking pattern of the donors and acceptors, varying degrees of conductivity can be achieved.[1−6] If the donors and acceptors assemble in segregated

Received: June 30, 2014
Published: September 22, 2014

   dx.doi.org/10.1021/ja506583k | J. Am. Chem. Soc. 2014, 136, 16185−16200

stacks, metallic or superconducting states can be achieved, whereas integrated stacks usually produce strong molecular magnets.

Given the interesting spectroscopic properties that they exhibit, an important application of metal-containing charge transfer complexes is their use in solar cells, specifically as photosensitizing dyes for wide band gap semiconductors.[7−9] This behavior has been demonstrated in recent years by several groups who have used Ru(II) and Pt(II) pyridyl complexes as photosensitizers for dye-sensitized solar cells (DSSCs) based on colloidal TiO_2.[8−10] Another potential application for modifications of such complexes is thin film-based organic photovoltaics (OPVs).[11] Typical OPV devices employ a donor sensitizer. The donor, a thermally evaporated thin film of a small molecule such as copper phthalocyanine (CuPc) or a solution-cast thin film of an organic polymer such as poly (3-hexyl)thiophene (P3HT), and an organic acceptor, typically a fullerene, interact in a separate or admixed layer.[12] Despite its historical lag in record performances versus DSSCs, the OPV technology is continuing to receive increasing attention because it has the potential to overcome some disadvantages of DSSCs. Record efficiency for DSSCs is now being held by a modular porphyrin-based sensitizer that attained 12.3% quantum efficiency,[10a] whereas the ruthenium dyes of *cis*-bis(isothiocyano)bis(2,2′-bipyridyl-4,4′-dicarboxylato)-ruthenium(II) have given maximum efficiencies of 9.57−11.2% in different reports for dyes with different counterions.[10b] Also recently tri(thiocyanto)(4,4′,4″-tricarboxy-2,2′:6′,2″-terpyridine)ruthenium(II) with organic coadsorbents has been reported with an efficiency of 11.4%.[10c] Disregarding tandem cells, OPV cells trail this efficiency with the state-of-the-art performance varying within 7−9% for single-junction nontandem devices processed via either solution casting or thermal evaporation.[13] DSSC disadvantages include loss of generated charge carriers due to recombination between the oxide semiconductor and the I^-/I^{3-} redox shuttle, corrosiveness and environmental hazard of the electrolyte solution (typically in acetonitrile), and inferior stability conferred by the liquid junction compared with the all-solid-state OPV device architecture. While the OPV technology has made significant strides within the past decade, one aspect of critically needed improvement is to develop sensitizers that exhibit significantly better overlap with the solar radiation than the current state-of-the-art materials. Figure 1 illustrates this limitation of the prototypical phthalocyanine and polythiophene (e.g., CuPc and P3HT, respectively) donors in contrast with two of the materials described in this work. Red and near-infrared (NIR) photons at wavelengths >650 nm constitute more than 50% of the solar radiation. Yet, this spectral region is notoriously excluded from the absorption range of P3HT and CuPc, which also exhibit depressions even within the visible region. Figure 1 indicates these limitations may be, in principle, overcome by materials described in this work, thus warranting further investigation toward their future utilization in OPVs. Here we describe the structural, magnetic, spectral, and electrochemical properties of Pt(II) square planar ambipolar complexes and binary adducts with nitrofluorenone acceptors. Following the report of experimental details and results is discussion of their suitability as sensitizers for DSSCs and OPVs.

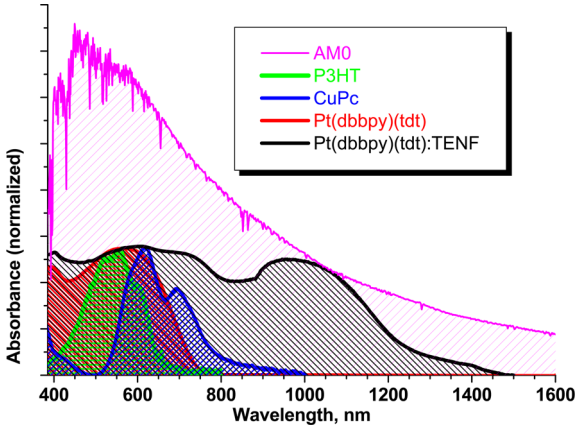

Figure 1. Overlap of solid-state absorption of different materials with the AM0 solar radiation.

In 2003, we reported new supramolecular assemblies containing inorganic complexes of general formula, M(dbbpy)(dmid) (M = Pt, Pd; dbbpy = 4,4′-di-*tert*-butyl-2,2′-bipyridine; $dmid^{2-}$ = 2-oxo-1,3-dithiole-4,5-dithiolate) and the nitrile organocyanide strong acceptors TCNQ, $TCNQF_4$, and TCNE, displaying optoelectronic properties of interest, both in solution and in the solid state.[14] We found, despite the absence of traditional tethering moieties such as carboxylates, phosphonates, or sulfonates on the pyridyl ring system, the peripheral cyanide group on the acceptor molecules can serve as an anchoring group. The attraction in solution and solid state is sufficient to tether the Pt moiety at the TiO_2 surface. Despite this interesting discovery, it was found these supramolecular systems suffered from reduced performance compared with the Ru(II)-pyridyl systems, an outcome likely due to the inability of organocyanide acceptors to inject an electron from their lowest energy states into the semiconductor's conduction band. Facile electron injection into the conduction band of the semiconductor occurs if the first reduction potential of the dye is more negative than the substrate. The first reduction potentials of the organocyanide acceptors ($E_{1/2}$ = +0.19, +0.54, and +0.17 V vs Ag/AgCl for TCNQ, $TCNQF_4$, and TCNE, respectively) suggest that none is more negative than the first reduction potential of the conduction band of TiO_2 (−0.6 V vs Ag/AgCl).[12] When the electron is injected from higher energy states of the donor, a fast recombination of the charge separated state between the donor and acceptor occurs rather than injection into the substrate, TiO_2; therefore, the solid adducts showed only weak absorptions in the NIR region due to the partially reduced nitrile acceptor species. In an attempt to overcome these DSSC and OPV limitations, we describe new supramolecular solids containing the inorganic complexes Pt(dbbpy)(tdt) and Pt(dmecb)(bdt) and the organic acceptors 2,7-dinitro-9-flourenone (DNF), 2,4,7-trinitro-9-flourenone (TRNF), and 2,4,5,7-tetranitro-9-flourenone (TENF); see Chart 1 for these molecular structures. The new binary complexes in this work are characterized by X-ray crystallography, cyclic voltammetry, infrared spectroscopy, UV−vis−NIR electronic absorption in solution and diffuse reflectance in the solid state, NMR spectroscopy, magnetic susceptibility, and solid-state tight binding simulations. This work is intended to elucidate some fundamental properties of the binary inorganic−organic complexes in the solid state and solution and also to serve as a backdrop for future investigations that pursue their potential in conducting and solar cell applications; a proof-of-concept for the potential of the latter application is shown based upon promising photoconductivity results for a thin film of Pt(dmecb)(bdt). The strong absorption bands throughout

dx.doi.org/10.1021/ja506583k | J. Am. Chem. Soc. 2014, 136, 16185−16200

Chart 1. Schematic Drawing of Pt(dbbpy)(tdt), Pt(dmecb)(bdt), and the Nitroflourenone Family of Acceptors Used in the Course of This Study

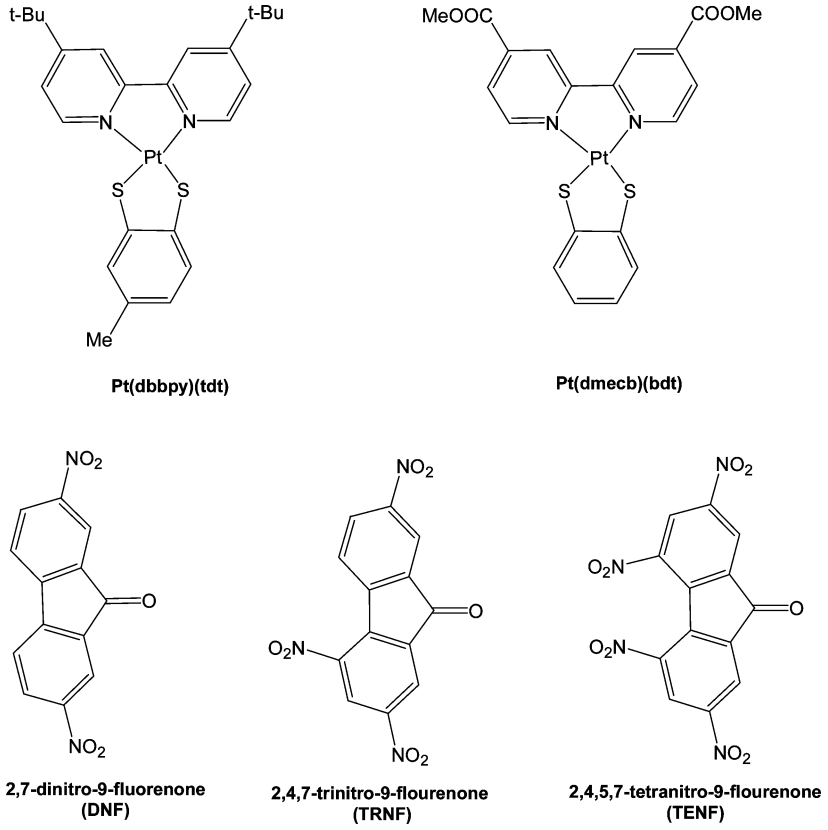

the visible and into the NIR region are favorable for solar cell applications.[7−14] The donor−acceptor columnar stacking and absence of discrete molecular states deduced from solid-state simulations are favorable for conducting applications,[1−6] including charge transport within the layer that contains the sensitizer in OPV devices.[11]

EXPERIMENTAL SECTION

All synthetic operations were performed under a nitrogen or argon atmosphere using standard Schlenk-line techniques. The reagent 2,7-dinitro-9-fluorenone (DNF) was purchased from TCI and used as received without further purification. In the initial phases of this work, the organic acceptors 2,4,7-trinitro-9-fluorenone (TRNF) and 2,4,5,7-tetranitrofluorenone (TENF) were provided by Prof. Alan Balch as previously obtained from Aldrich (no longer available) and were used without additional purification. Later these two acceptors were synthesized by published procedures and purified by chromatography.[15] Benzene was distilled over tetraglyme-stabilized potassium/benzophenone, and dichloromethane was distilled over P_2O_5 or CaH_2. The starting platinum precursor material, K_2PtCl_4, was purchased from Pressure Chemical Co. and reacted with 4,4′-di-*tert*-butyl-2,2′-bipyridine (dbbpy) or 4,4′-dimethoxy-2,2′-bipyridine (dmecb) to prepare (dbbpy)$PtCl_2$ or (dmecb)$PtCl_2$ based on a published procedure.[16] The 4,4′-dimethoxy-2,2′-bipyridine (dmecb) ligand was prepared following a published method[17a] and recrystallized from hot methanol, and the purity of the colorless crystals verified by melting point comparison to a reported literature value (mp 209.5−211 °C).[17b] Pt(dbbpy)(tdt) and Pt(dmecb)bdt were prepared according to literature procedures.[18] The purity of Pt(dmecb)bdt was verified by elemental analysis (QTI) [Anal. Calcd (%): C, 39.54; H, 2.65; N, 4.61. Found: C, 39.23; H, 2.47; N, 4.71] and ^{1}H NMR (400 MHz, DMSO-d_6) [δ 9.32 (2 H, d, J = 5.9), 9.10 (2 H, s), 8.16 (2 H, dd, J = 5.8,1.8 Hz), 7.26 (2 H, dd, J = 5.7,3.2 Hz), 6.75 (2 H, dd, J = 5.7,3.2 Hz), 4.00 (6 H, s)].

Crystal Growth. The compounds [Pt(dbbpy)(tdt)][DNF] (**1**), [Pt(dbbpy)(tdt)][TRNF] (**2**), and [Pt(dbbpy)(tdt)]$_2$[TENF] (**3**) were prepared by layering CH_2Cl_2 solutions of Pt(dbbpy)(tdt) with solutions of the organic acceptor in a CH_2Cl_2/C_6H_6 solution. The flask, covered with aluminum foil, was left to sit undisturbed for approximately 1 week. The resulting dark blue/black solution slowly evaporating under nitrogen atmosphere yielded dark blue/black needles of the three materials. The crystallized supramolecular systems **1**−**3** were obtained using a 2:1 ratio of D/A molecules (D = Pt(dbbpy)(tdt) donor; A = nitrofluorenone acceptor) to attain the given empirical compositions so only **3** followed the mixing ratio. A second polymorph of the complex between Pt(dbbpy)(tdt) and TENF (**4**) was obtained using the same preparative conditions as **1**−**3**, with the exception of using a 1:1 D/A ratio instead of 2:1. The solids appear air- and moisture-stable. The resulting solid products maintain their dark blue/black colors under room light and ambient atmosphere. The crystalline quality for the samples diminishes over a period of a few days due to loss of benzene from the crystals.

[Pt(dbbpy)(tdt)][DNF]·0.5C_6H_6 (1·0.5C_6H_6). Under a nitrogen atmosphere, a dark purple solution of Pt(dbbpy)(tdt) (0.0154 g, 2.4 × 10^{-4} mol) in 5 mL of CH_2Cl_2 was layered with a pale yellow solution of DNF (0.0034 g, 1.2 × 10^{-4} mol) in 10 mL of a 1:1 solution of CH_2Cl_2/benzene. The tube, carefully covered in aluminum foil, was left undisturbed for 1 week. The resulting black solution slowly evaporating under nitrogen resulted in the formation of dark blue/black needles of [Pt(dbbpy)(tdt)][DNF]·0.5C_6H_6 (**1·0.5C_6H_6**) after 1 week.

[Pt(dbbpy)(tdt)][TRNF]·C_6H_6 (2·C_6H_6). In a manner similar to that used for **1**, a dark purple solution of Pt(dbbpy)(tdt) (0.0154 g, 2.4 × 10^{-4} mol) in 5 mL of CH_2Cl_2 was layered with a pale yellow solution of TRNF (0.0039 g, 1.2 × 10^{-4} mol) in a 1:1 solution of CH_2Cl_2/benzene. Dark blue/black needles of [Pt(dbbpy)(tdt)]-[TRNF]·C_6H_6 (**2·C_6H_6**) formed within 10 days.

[Pt(dbbpy)(tdt)]$_2$[TENF]·2C_6H_6 (3·2C_6H_6). By using a procedure similar to that used to prepare **1** and **2**, Pt(dbbpy)(tdt) (0.0154 g,

dx.doi.org/10.1021/ja506583k | J. Am. Chem. Soc. 2014, 136, 16185−16200

2.4×10^{-4} mol) and TENF (0.0045 g, 1.2×10^{-4} mol) were combined and isolated as dark blue/black needles of $[Pt(dbbpy)(tdt)]_2[TENF]\cdot 2C_6H_6$ ($\mathbf{3\cdot 2C_6H_6}$) after 7 days.

[Pt(dbbpy)(tdt)][TENF]·0.5C$_6$H$_6$ (4·0.5C$_6$H$_6$). By using an analogous synthetic procedure as described for **1**–**3**, a 1:1 ratio of Pt(dbbpy)tdt and TENF was combined and slowly evaporated under argon for several days to a final volume of 5 mL, ultimately producing black crystals.

[Pt(dmecb)bdt][*x*NF] where *x*NF is DNF, TRNF, or TENF. By using the same procedures as the analogous **1**, **2**, and **4**, black-blue powders were collected after slow evaporation of solvent over a period of several days.

Single Crystal X-ray Structural Studies. X-ray data for $[Pt(dbbpy)(tdt)][DNF]\cdot 0.5C_6H_6$ ($\mathbf{1\cdot 0.5C_6H_6}$), $[Pt(dbbpy)(tdt)][TRNF]\cdot C_6H_6$ ($\mathbf{2\cdot C_6H_6}$), and $[Pt(dbbpy)(tdt)]_2[TENF]\cdot 2C_6H_6$ ($\mathbf{3\cdot 2C_6H_6}$) were collected on a Bruker D8 GADDS system at 110 ± 2 K with graphite monochromated Cu Kα (λ = 1.54178 Å) radiation at the X-ray diffraction facility at Texas A&M University. The data were corrected for Lorentz and polarization effects. The Bruker SAINT software package was used to integrate the frames, and the data were corrected for absorption using the SADABS program.[19,20] The structures were solved by direct methods by the use of the SHELXS-97 program in the Bruker SHELXTL v5.1 software package.[21,22] The final refinement was carried out with anisotropic thermal parameters for all non-hydrogen atoms except for the atoms of the interstitial solvent molecules. Hydrogen atoms were placed in calculated positions. The final crystal structural representations were generated using the XSEED program.[23]

X-ray data for $[Pt(dbbpy)(tdt)][TENF]\cdot 0.5C_6H_6$ ($\mathbf{4\cdot 0.5C_6H_6}$) were collected on a Bruker SMART APEX II CCD-based diffractometer and a Mo Kα fine-focus sealed tube (λ = 0.71073 Å) with a graphite monochromator operated at 50 kV, 30 mA at 100 K at the University of North Texas.

The data frames for each compound were integrated with the available APEX2 software using a narrow-frame algorithm.[24] Structures were solved and refined using the SHELXTL program package.[24] The dbbpy ligand in **4**, disordered over two positions, was refined accordingly with distance constraints. All non-hydrogen atoms were refined anisotropically. Hydrogen atoms were assigned to calculated positions and allowed to ride on the attached carbon atoms in final structure refinements. The molecular structures for all compounds were checked using PLATON.[25] Crystallographic parameters for ($\mathbf{1\cdot 0.5C_6H_6}$), ($\mathbf{2\cdot C_6H_6}$), ($\mathbf{3\cdot 2C_6H_6}$), and ($\mathbf{4\cdot 0.5C_6H_6}$) are listed in Tables 1 and 2. CCDC files 669761–669764 contain the supplementary crystallographic data for this paper. These data can be obtained free of charge from the Cambridge Crystallographic Data Centre via www.ccdc.cam.ac.uk/data_request/cif. Bond distances for all compounds are presented in the Supporting Information.

See CIF files in the Supporting Information for additional crystallographic details, including responses to alerts in the CheckCIF files.

Physical Measurements. Infrared spectra for **1**, **2**, and, **3** in the 4800–400 cm^{-1} range were recorded on a Nicolet 740 FT-IR spectrophotometer; spectra in the the far IR range (1600–50 cm^{-1}) were recorded on a computer controlled Nicolet 750 FT-IR spectrophotometer equipped with a TGS/PE detector and silicon beam splitter at 2.0 or 4.0 cm^{-1} resolution. The IR spectra for **4**, Pt(dbbpy)tdt, and 2,4,5,7-tetranitrofluorenone were collected on a PerkinElmer Spectrum B (CsI optics) in the range of 4000–400 cm^{-1} for an average of 16 scans per sample, at a resolution of 1 cm^{-1}. Background pellet consists of 0.2000 g of FT-IR grade KBr (Fluka), and the sample pellet consists of approximately 1–2% sample, ground with KBr to equal 0.20 g.

Cyclic voltammetric measurements were carried out on **1**–**3** at a scan rate of 100–200 mV/s using a CH Instruments electrochemical analyzer in 0.1 M solutions of $[n\text{-}(Bu)_4N][PF_6]$ in CH_2Cl_2 at a Pt disk working electrode with a Ag/AgCl reference and a Pt counter electrode.

UV–vis–NIR electronic absorption and diffuse reflectance spectral measurements were carried out using a PerkinElmer Lambda 900 spectrophotometer in Suprasil quartz cuvettes with 1, 10, and 100 mm path lengths. The solid reflectance data were collected using the LabSphere integrating sphere accessory to the Lambda 900 spectrophotometer. The UV–vis–NIR absorption spectra for complexes **1**–**3** were performed at room temperature using a given amount of Pt(dbbpy)tdt and adding, in stoichiometric amounts, the corresponding nitrofluorenone from a stock solution, then diluting the mixture to 25 mL. The resulting solutions were used immediately to

Table 1. X-ray Crystallographic and Refinement Data for 1 and 2

compound	[Pt(dbbpy)(tdt)][DNF]·0.5C$_6$H$_6$ (**1**)	[Pt(dbbpy)(tdt)][TRNF]·C$_6$H$_6$ (**2**)
formula	$C_{41}H_{39}N_4O_5PtS_2$	$C_{44}H_{41}N_5O_7PtS_2$
formula weight	926.97	1011.03
space group	$P\bar{1}$	$Fdd2$
a, Å	11.298(2)	52.430(6)
b, Å	13.599(3)	48.844(6)
c, Å	13.964(3)	6.799(8)
α, deg	75.51(3)	90
β, deg	86.77(3)	90
γ, deg	69.05(3)	90
V, Å^3	1938.6(7)	17410(4)
Z	2	16
μ, mm^{-1}	3.776	7.381
temp	100(2)	100(2)
reflns collected	8504	5787
reflns $I > 2\sigma$	7303	4708
R1[a]	0.0352	0.0556
wR2[b]	0.0813	0.1371
GOF[c]	1.099	1.017

[a] $R1 = \sum||F_o| - |F_c||/\sum|F_o|$. [b] $wR2 = [\sum[w(F_o^2 - F_c^2)^2]/\sum[w(F_o^2)^2]]^{1/2}$. [c] Goodness-of-fit $= [\sum w(|F_o| - |F_c|)^2/(N_{obs} - N_{parameter})]^{1/2}$.

Table 2. X-ray Crystallographic and Refinement Data for 3 and 4

compound	[Pt(dbbpy)(tdt)]$_2$[TENF]·2C$_6$H$_6$ (**3**)	[Pt(dbbpy)(tdt)][TENF]·C$_6$H$_6$ (**4**)
formula	$C_{75}H_{76}N_8O_9Pt_2S_4$	$C_{41}H_{37}N_6O_9PtS_2$
formula weight	1751.86	1016.98
space group	$P2(1)/n$	$P2(1)/n$
a, Å	11.257(2)	23.128(2)
b, Å	26.004(5)	7.164(6)
c, Å	24.165(5)	25.474(2)
α, deg	90	90
β, deg	92.19(3)	109.19(2)
γ, deg	90	90
V, Å^3	7069(2)	7069(2)
Z	4	4
μ, mm^{-1}	8.918	3.690
temp	100(2)	100(2)
reflns collected	8873	41047
reflns $I > 2\sigma$	2834	7294
R1[a]	0.0931	0.0480
wR2[b]	0.1707	0.1076
GOF[c]	0.919	1.041

[a] $R1 = \sum||F_o| - |F_c||/\sum|F_o|$. [b] $wR2 = [\sum[w(F_o^2 - F_c^2)^2]/\sum[w(F_o^2)^2]]^{1/2}$. [c] Goodness-of-fit $= [\sum w(|F_o| - |F_c|)^2/(N_{obs} - N_{parameter})]^{1/2}$.

dx.doi.org/10.1021/ja506583k | J. Am. Chem. Soc. 2014, 136, 16185–16200

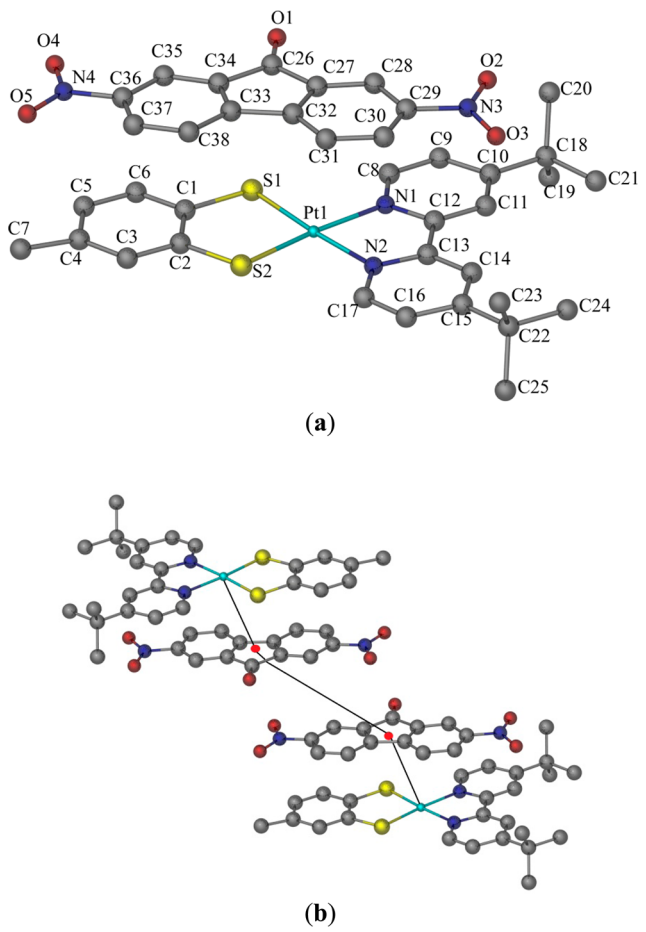

Figure 2. (a) X-ray crystal structure for [Pt(dbbpy)(tdt)][DNF]·$0.5C_6H_6$ (**1·0.5C$_6$H$_6$**) and (b) the contents of the unit cell illustrating the one-dimensional stacking motif and interactions involving the donor and acceptor molecules at the platinum atom and calculated centroid (red dot), respectively. Hydrogen atoms and interstitial benzene molecules have been omitted for the sake of clarity.

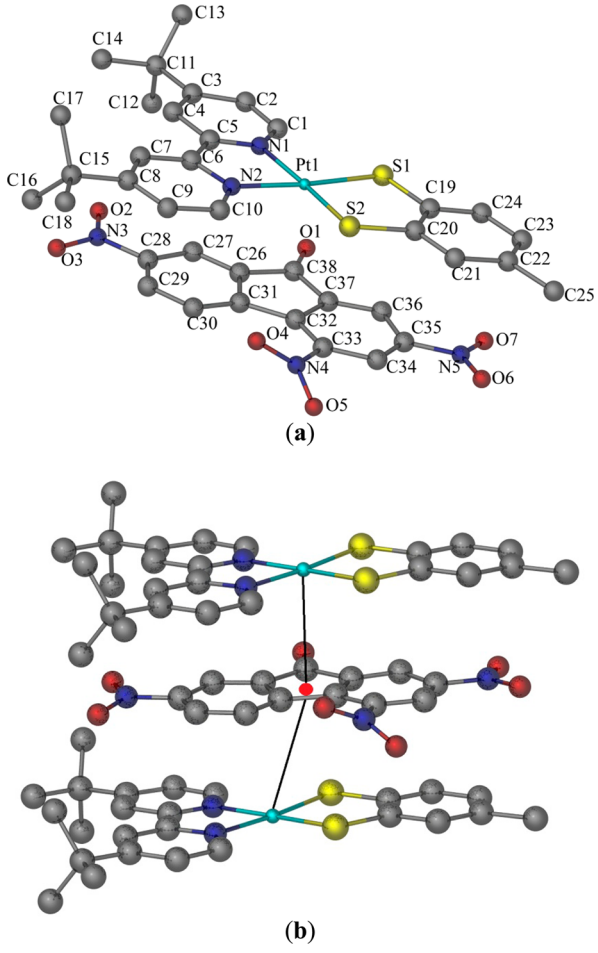

Figure 3. (a) X-ray crystal structure of [Pt(dbbpy)(tdt)][TRNF]·C_6H_6 (**2·C$_6$H$_6$**) and (b) illustrates the one-dimensional stacking motif and interactions between the donor and acceptor molecules involving the platinum atom and calculated centroid (red dot) respectively. Hydrogen atoms and interstitial benzene molecules have been omitted for the sake of clarity.

collect the spectral data. For the solid-state spectral data (diffuse reflectance), the solutions used for UV−vis−NIR studies were mixed, and the volume was reduced under vacuum. The solution was then reconstituted to 25 mL by the addition of dichloromethane and benzene. The solutions were then slowly evaporated under argon. The resultant solid crystalline product was collected and placed on a Whatman filter paper. The filter paper was used as the substrate for reflectance measurements for the solids.

NMR spectra were collected on a Varian VNMRS 500 MHz spectrometer. The samples were prepared by dissolving them in $CDCl_3$ and placing them in a 5 mm NMR tube (Wilmad). One-dimensional ^{1}H spectra were acquired with 265 scans and 1.0 s relaxation delay. Two-dimensional ^{1}H NOESY (nuclear Overhauser effect spectroscopy) spectra were acquired with 0.7 s mixing time, 1.0 s relaxation delay, and 128 s dimension increments with 128 scans in each increment. The spectra were referenced to the solvent peaks for $CDCl_3$ (7.26 ppm).

Photoconductivity Measurements. A Schottky diode with the structure glass/ITO/Pt(dmecb)(bdt) (20 nm)/Mg:Ag, 1:10 (200 nm) was fabricated by sequential thermal evaporation using a multisource programmable Trovato thermal deposition system. The active layer was evaporated slowly at a rate of 0.25 Å/s. Quartz crystal oscillators were used to monitor the film thicknesses, which were calibrated *ex situ* using a profilometer (VEECO DEKTAK VIII), whereas the Mg/Ag ratio in the cathode was evaluated via EDAX measurements. Prior to device fabrication, the glass/ITO substrates were cleaned by sonication in acetone then methanol for 15 min, and afterward subjected to an oxygen plasma treatment for ITO surface conditioning. A Keithley 2420 source-measure unit was used for quantitative electrical characterization for both the dark current and photocurrent using a xenon lamp as a solar simulator; this apparatus is factory-calibrated. All measurements were performed at room temperature.

Solid-State Simulations. The computational modeling utilized the extended Hückel tight binding (EHTB) method for which standard parameters were used within the YAeHMOP software package.[26,27] The off-diagonal elements of the Hamiltonian were evaluated with the Wolfsberg−Helmholtz formula.[28] Numerical integrations over the symmetry-unique section of the Brillouin zone of the three-dimensional structure of [Pt(dbbpy)(tdt)][TENF] (the 1:1 polymorph, complex **4**) were performed using a set of 40 k-points.[26−28]

RESULTS AND DISCUSSION

X-ray Crystallographic Studies. Figures 2−5 show the crystal structures of the crystalline adducts **1**−**4**, respectively. The crystallographic data suggest that all four compounds exhibit significant donor−acceptor (charge-transfer) interactions in the solid state, as judged by interplanar distances between D and A molecules that are shorter than 3.75 Å, which are well within the range reported for $\pi-\pi$, d−π, and electrostatic donor−acceptor interactions.[1−6] These distances are similar to those intermolecular distances observed for partially oxidized

dx.doi.org/10.1021/ja506583k | J. Am. Chem. Soc. 2014, 136, 16185−16200

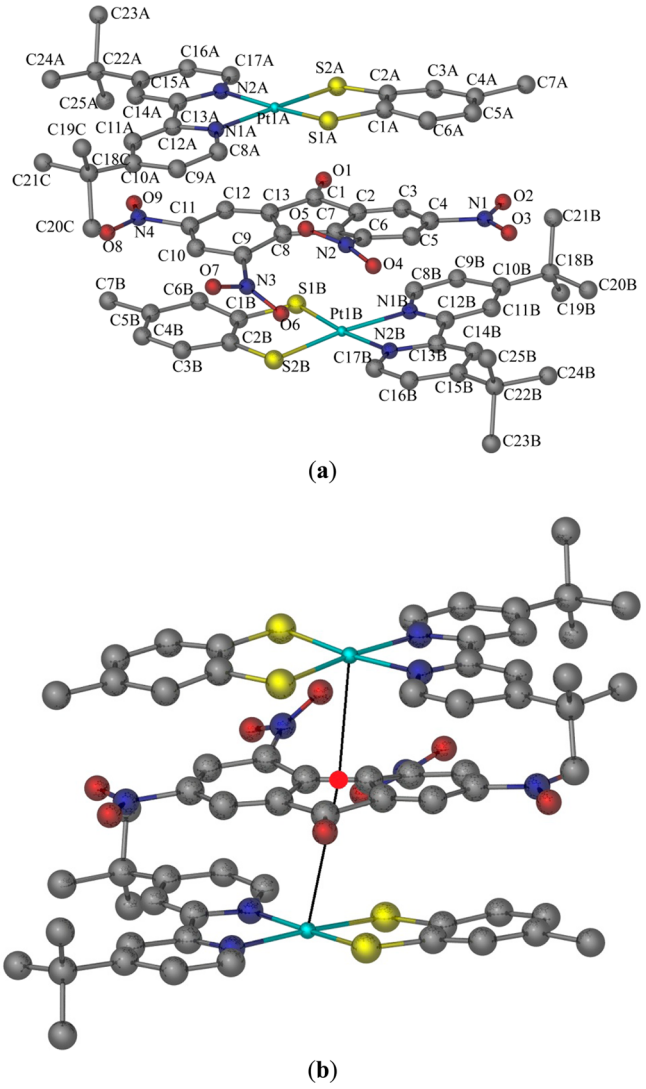

(a)

(b)

Figure 4. (a) X-ray crystal structure of $[Pt(dbbpy)(tdt)]_2[TENF]\cdot 2C_6H_6$ (**3·2C$_6$H$_6$**) and (b) the contents of the unit cell illustrating the one-dimensional stacking motif and interactions between the donor and acceptor molecules at the platinum atom and calculated centroid (red dot), respectively. Hydrogen atoms and interstitial benzene molecules have been omitted for the sake of clarity.

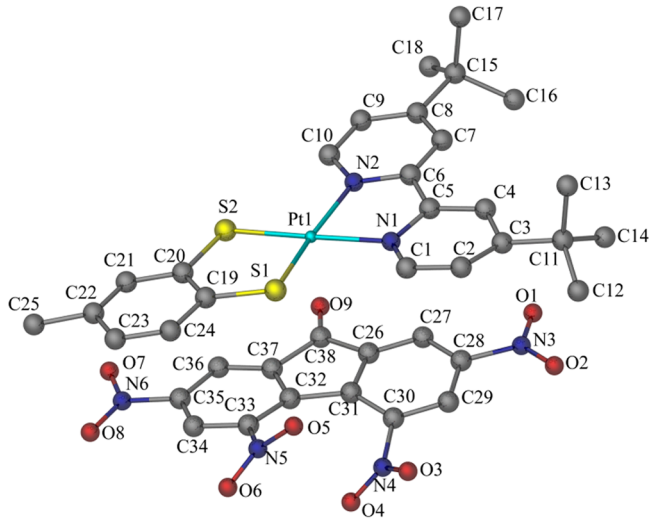

(a)

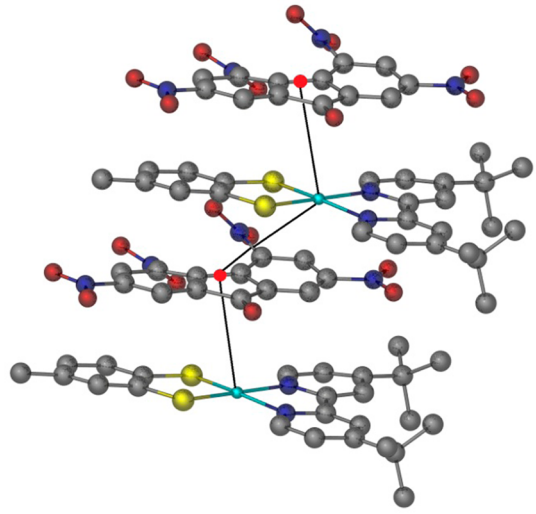

(b)

Figure 5. (a) X-ray crystal structure of $[Pt(dbbpy)(tdt)][TENF]\cdot C_6H_6$ (**4·0.5C$_6$H$_6$**) and (b) the contents of the unit cell illustrating the one-dimensional stacking motif and interactions between the donor and acceptor molecules at the platinum atom and calculated centroid (red dot), respectively. Hydrogen atoms and interstitial benzene molecules have been omitted for the sake of clarity.

derivatives of tetrathiafulvalene (TTF) in various highly conducting systems in which intermolecular distances between neighboring donor molecules within 3.75 Å are indicative of partial charge transfer.[29] The same situation holds for the [Pt(dbbpy)dmid][TCNQ] stacks previously reported by us, which exhibit close interplanar distances with strong evidence for partial charge transfer inferred from ν_{C-N} IR data, as well as magnetic meaurements.[14]

The molecular units in **1** crystallize in the triclinic space group $P\bar{1}$. The donor and acceptor molecules form supramolecular stacks in a 2:2 D/A pattern in each column. The DNF acceptor molecule is situated directly above the donor, which allows for improved orbital overlap between the acceptor and the M−tdt donor unit whose combined orbital contribution comprises the HOMO for the M(diimine)-(dithiolate) donor molecules.[18] The unique stacking consists of dimeric interactions between two acceptors and two donors. This structure is rare in that 2:1 or 1:1 D/A patterns are common but a 2/2 D:A pattern has not been observed previously. The X-ray crystal structure for **1** and its unit cell projection illustrating the one-dimensional packing in the solid state are shown in Figure 2.

Compounds **2** and **3** crystallize in the space groups *Fdd*2 and $P2_1/n$, respectively. Both systems exhibit overlap between the donor and acceptor molecules but with a different molar ratio. The X-ray structure of **2** reveals a 1:1 D/A stacking pattern, whereas **3** exhibits a 2:1 D/A pattern in which the TENF molecule is sandwiched between dimeric donor complexes. In the absence of the TENF acceptor, the donor molecules are stacked head-to-tail in an eclipsed manner. The structure of **4** is similar to the stacking pattern of **2** as the ratio of D/A molecules is 1:1. The crystal structures show one-dimensional stacking projections for **1**−**4**, as depicted in Figures 2−5.

The intermolecular distances for **1**−**4** are listed in Table 3. Structure **4** exhibits two distinct D/A contacts, a short D/A

dx.doi.org/10.1021/ja506583k | J. Am. Chem. Soc. 2014, 136, 16185−16200

Table 3. Intermolecular Distances Representing D−A Interactions for 1−4

	d_{D-A}[a] (Å)	d_{A-A}[b] (Å)	d_{D-D}[c] (Å)
[Pt(dbbpy)(tdt)][DNF]·0.5C_6H_6 (**1**·0.5C_6H_6)	3.75	5.15	7.09
[Pt(dbbpy)(tdt)][TRNF]·C_6H_6 (**2**·C_6H_6)	3.33		
	3.62		
[Pt(dbbpy)(tdt)]$_2$[TENF]·2C_6H_6 (**3**·2C_6H_6)	3.50	4.72	
	3.52		
[Pt(dbbpy)(tdt)][TENF]·0.5C_6H_6 (**4**·0.5C_6H_6)	3.47		
	4.48		

[a]Distances between platinum atom and calculated centroids. [b]Distances between calculated centroids. [c]Distances between platinum atoms.

interaction of 3.47 Å from the Pt1 atom to the centroid of the 13-atom nitrofluorenone fused-ring and a long D/A interaction of 4.48 Å along the crystallographic *b*-direction. The elongation of the D/A distance may be due to the insertion of a benzene molecule between every other pair of D/A moieties. The inclusion of a benzene molecule in **4** also causes disorder in the dbbpy ligand. In contrast, each of the three other structures exhibits a single significant D/A contact within 3.33−3.75 Å. These distances are similar to those reported by the Balch group for Au(I) trimeric species with DNF, TRNF, and TENF (3.45−3.48 Å).[30] Our previous studies for Pt(diimine)-(dithiolate) complexes with the electron acceptors TCNE, TCNQ, and $TCNQF_4$ reveal D/A distances ranging from 3.21 Å for TCNE to 3.49 Å for TCNQ.[14] Another study by the Fackler group revealed that adducts between Au(I) cyclic trinuclear donor complexes with TCNQ acceptor exhibited D/A intercentroid distance of 3.96 Å.[31] These D/A complexes all display similar distances indicative of significant molecular interactions in the solid state. In addition to intimate distances, the stacks are kinked, causing the D and A associating molecules to be misaligned to various degrees. The 1:1 structure in **2**, however, is the most symmetrical extended structure with the greatest spatial overlap of D and A molecules in extended one-dimensional chains. The Supporting Information files contain the qualifying details.

Electrochemistry. Cyclic voltammetric studies of **1**−**3** reveal two irreversible oxidations at +0.49 and +0.90 V (vs Ag/AgCl as is the case for all electrochemical data in this work). These oxidations are attributed to the M−tdt unit.[18] Solutions of **1** show two reversible reductions at −0.70 and −0.90 V, attributed to the two reductions of the DNF acceptor. A third irreversible reduction at −1.30 V is assigned to a reduction of the dbbpy ligand. Compound **2** exhibits irreversible oxidations similar to those in **1**. Reversible reductions, presumably acceptor-based, occur at −0.42 and −0.68 V. The experimental cutoff for the electrochemical analysis of **2** was limited to −1.0 V, thus preventing the observation of other reduction processes. Compound **3** exhibits similar anodic behavior to that for the previous systems and begins to show cathodic behavior similar to that for the pure TENF acceptor with the first and second reversible reductions occurring at +0.18 and −0.25 V, respectively. In a fashion similar to **2**, the electrochemical range of the experiment for **3** was halted at −1.0 V, again preventing the observation of other reduction processes. It is important to note that, for all of the adduct systems, when the electrochemical experiments are carried out in dichloromethane solution, the systems display electrochemical behavior similar to the individual starting materials, Pt(dbbpy)tdt and the corresponding acceptor. Literature values for the Pt(dbbpy)tdt donor are $E_p(ox)$ = 0.589 V and $E_{1/2}(red)$ = −1.198 V,[18] whereas for the acceptors, the following values are found: DNF, $E_{1/2}(red)$ = −0.68, −0.84 V; TRNF, $E_{1/2}(red)$ = −0.42, −0.67 V; TENF, +0.14 and −0.42 V (all converted to values vs Ag/AgCl for comparison with our values).[32] Since the electrochemical measurements for **1**−**3** are carried out in solution, the packing arrangement observed in the solid state structures is not preserved. The electronic spectra, discussed below, in 10 cm cuvettes to increase the detectability of weaker absorptions, show weak NIR absorption bands indicating that the adduct equilibrium constant is relatively small. Thus, the concentration of the binary D/A adduct in solution is very low relative to the separate components, and it cannot be observed by solution electrochemistry. A summary of the electrochemical potentials observed from **1**−**3** is presented in Table 4. Since the

Table 4. Summary of Electrochemical Potentials (V) for 1·0.5C_6H_6, 2·C_6H_6, and 3·2C_6H_6[a]

compound	$E_p(ox)$, donor	$E_{1/2}(red)$, acceptor
[Pt(dbbpy)(tdt)][DNF]·0.5C_6H_6 (**1**·0.5C_6H_6)	+0.49	−0.70
	+0.90	−0.90
[Pt(dbbpy)(tdt)][TRNF]·C_6H_6 (**2**·C_6H_6)	+0.50	−0.42
	+0.88	−0.68
[Pt(dbbpy)(tdt)]$_2$[TENF]·2C_6H_6 (**3**·2C_6H_6)	+0.48	+0.18
	+0.86	−0.25

[a]Values are volts vs Ag/AgCl, Pt disk electrode in 0.1 M $TBAPF_6$/CH_2Cl_2 at a scan rate of 100 mV/s. Experimental runs were stopped at a lower limit of −1.0 V. This prevented the observation of the dbbpy ligand-based reduction and the observation of an additional cathodic response from the TRNF and TENF acceptors.

voltammograms show features indicative of the oxidation and reduction of the pure donor and acceptor components, respectively, **4** was not subjected to electrochemical analysis because the results should be similar to those observed for **3**.

Infrared Spectral Studies. The infrared spectra for the stacks versus the free molecules are shown in Figure 6. The

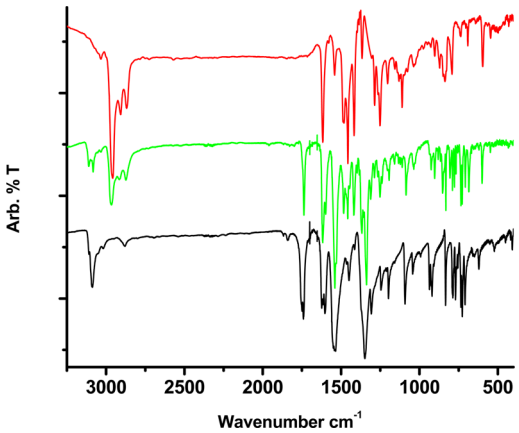

Figure 6. Infrared spectrum for Pt(dbbpy)(tdt) (top), stack **4** (middle), and TENF (bottom).

most notable change is a shift in the ν_{C-O}, and ν_{N-O} modes (Supporting Information, Figures S1−S3). The solid state stacking implies that charge transfer is possible as previously

dx.doi.org/10.1021/ja506583k | J. Am. Chem. Soc. 2014, 136, 16185−16200

demonstrated by our work involving nitrile acceptors.[14] Significant shifts occur in the C═O stretching frequency in the TENF stack **4**. As one would expect, there are no absorptions in this region for the Pt moiety. However, free TENF exhibits two very strong absorption bands at 1749 and 1741 cm^{-1}. The stacked compound no longer shows two bands for the free TENF because only one band is seen at 1737 cm^{-1}, which represents a lower frequency mode than either band in free TENF. The C═C bands for the free TENF appear at 1614, 1623, and 1603 cm^{-1}. The 1614 and 1623 cm^{-1} features interfere with the Pt complex band at 1617 cm^{-1} in the stack, but the 1603 cm^{-1} band shows a red shift to 1598 cm^{-1}.

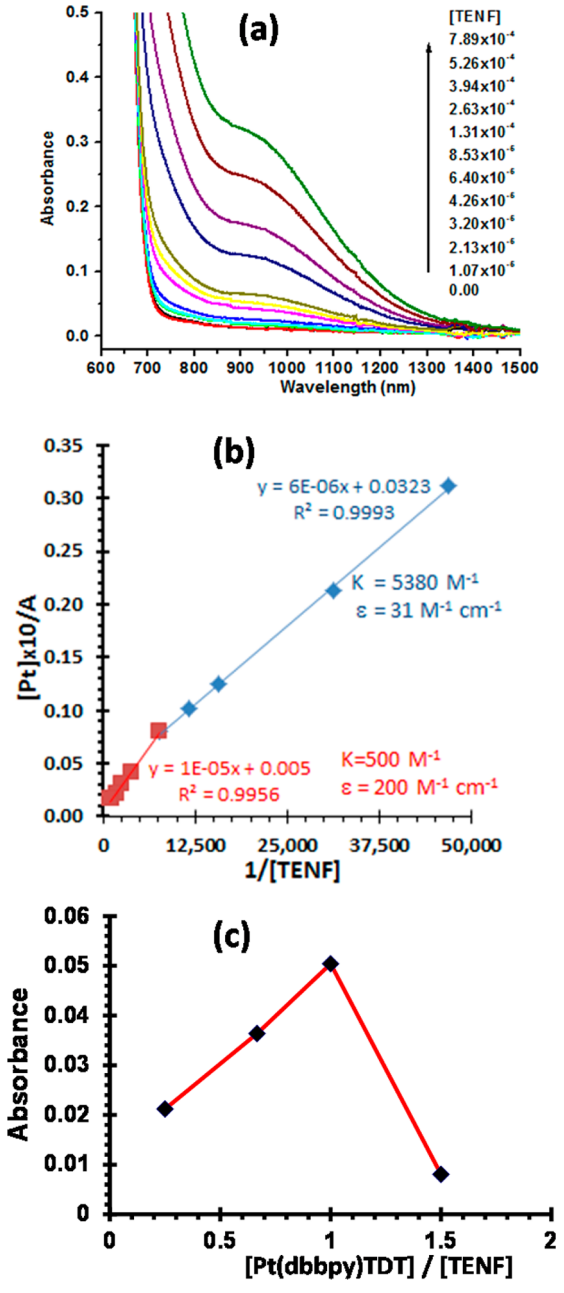

Figure 7. (a) Absorption spectra showing the DACT band growth during the titration experiment for [Pt(dbbpy)(tdt)][TENF] in CH_2Cl_2 using a 10 cm cuvette at room temperature. (b) Benesi–Hildebrand plot of the spectral changes measured at 950 nm. (c) Job plot for the spectral changes measured at 950 nm.

The most significant changes are observed in the NO_2 bands at 1549–1534 and 1349 cm^{-1}. The broad peak at ca. 1544 cm^{-1} in the free acceptor is sharper for the stacked product with a maximum at 1539 and a shoulder at 1530 cm^{-1}. The acceptor peak at 1349 cm^{-1} is shifted and more resolved in the stack with the maximum shifting to 1337 cm^{-1}. These IR data clearly suggest the influence of charge transfer in this system. This situation is similar to what is observed for monoreduced TCNQ and $TCNQ^{\delta-}$, where a red shift of the CN stretch was reported.[14,33] We are unable to estimate the partial charge delocalization in these systems, due to a lack of literature correlations of IR frequencies for nitrofluorenone systems similar to those known for $TCNQ^{\delta-}$ systems.[29,33]

UV–Vis–NIR Electronic Absorption Spectral Studies. Figures 7–9 and Supporting Information, Figures S4–S7, show electronic spectral data that provide insights into how D/A interactions affect the electronic structure of the binary adducts in both the solid state and solution. At one extreme, the UV–vis–NIR data for **1** show very little variation in the low energy region beyond the CT band of the Pt(dbbpy)tdt (Supporting Information, Figures S4 and S5). The 1 cm cuvette measurements reveal little variation in the extinction coefficients of the Pt(dbbpy)tdt complex, which would be expected if significant interactions were occurring in solution. In the solid state, there is also no evidence of a D/A interaction between DNF and Pt(dbbpy)tdt. The solid state reflectance data for the powder sample reveal no evidence for a new band in the low energy region below the CT band of Pt(dbbpy)tdt.

Antithetically, the spectral data clearly indicate that there is a much stronger interaction between the TRNF or TENF acceptor molecules and the Pt(dbbpy)tdt donor complex. The TENF adduct exhibits an emerging band at 950 nm growing progressively more intense with incremental addition of TENF (Figure 7a). The titration data were fit using the same method as that used for complex **2** (Figure 7b). The magnitude of the equilibrium constant calculated as 5380 M^{-1} is much higher

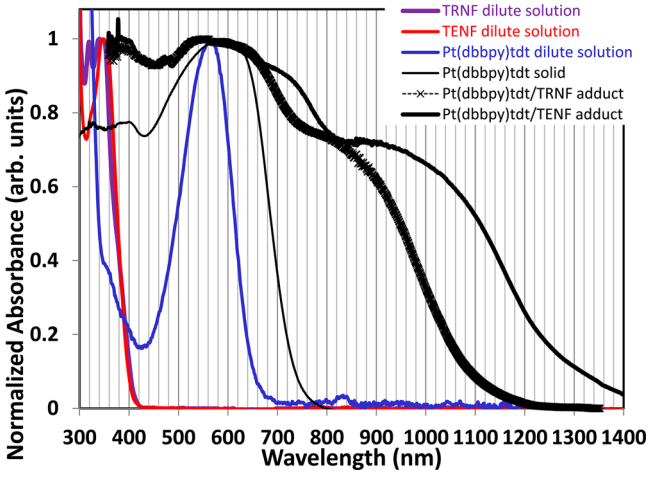

Figure 8. Solid state diffuse reflectance data (top trio) for **4** (top), **2** (middle), and Pt(dbbpy)(tdt) (bottom) showing the strong DACT absorptions in the NIR region. For comparison, normalized spectra for the dilute solutions (~10^{-5} M) of Pt(dbbpy)tdt, TRNF, and TENF are presented as the lower trio. For dilute solutions, the curves have been normalized for TRNF, TENF, and Pt(dbbpy)tdt at 340, 347, and 566 nm, respectively. For the solids, the curves have been normalized for Pt(dbbpy)tdt, TRNF adduct, TENF adduct at 599, 547, and 550 nm, respectively.

dx.doi.org/10.1021/ja506583k | J. Am. Chem. Soc. 2014, 136, 16185–16200

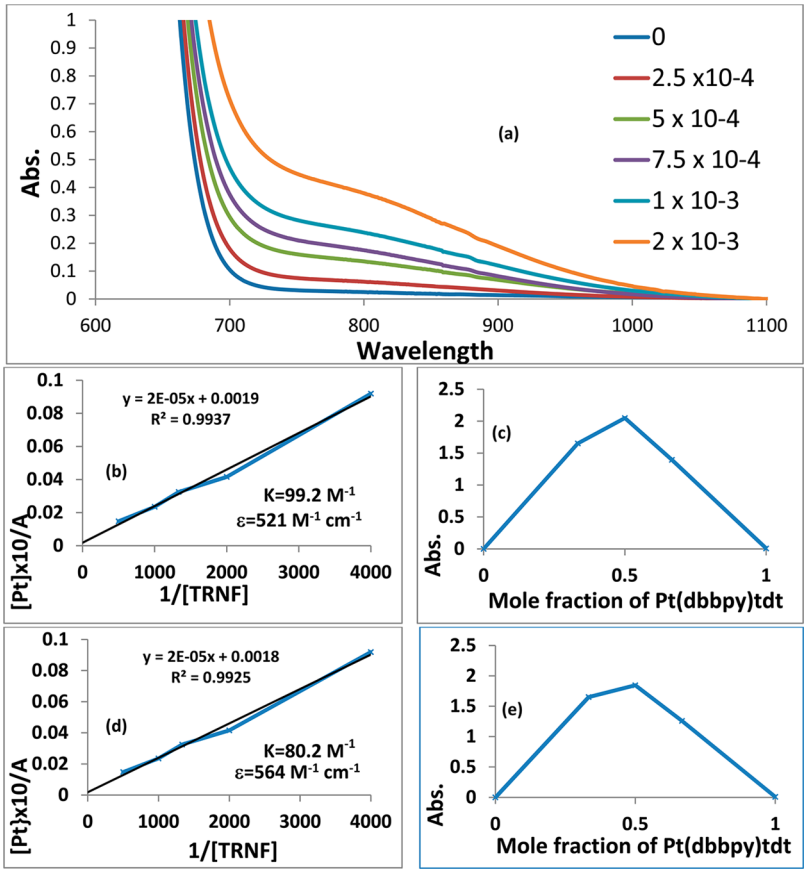

Figure 9. (a) Absorption spectra showing DACT band growth during the titration experiment for [Pt(dbbpy)(tdt)] and [TRNF] in CH_2Cl_2 using a 10 cm cuvette at room temperature. [Pt(dbbpy)tdt] = 5×10^{-4} M. (b) Benesi–Hildebrand plot of the spectral changes at 800 nm. (c) Job plot for the spectral changes at 800 nm. [Pt(dbbpy)tdt + TRNF] = 5×10^{-4} M. (d) Benesi–Hildebrand plot of the spectral changes at 825 nm. (e) Job plot for the spectral changes at 825 nm. [Pt(dbbpy)tdt + TRNF] = 5×10^{-4} M.

than that found for **2**, indicative of the strong attraction of TENF to the electron-rich Pt(dbbpy)(tdt). The Job plot in Figure 7c clearly indicates, even in solution, that the 1:1 ratio remains dominant. The adduct exhibits an extinction coefficient of 31 M^{-1} cm^{-1}. In the solid spectra, this absorption becomes nearly as intense as the donor absorptions according to the corresponding diffuse reflectance spectra (Figure 8). Analogous data were found for the [Pt(dbbpy)(tdt)][TRNF] binary system. The absorption spectra for the titration of Pt(dbbpy)-(tdt) with TRNF are presented as Figure 9. The data feature the growth of a new absorption feature in the 825 nm region. This band becomes more intense with increasing concentration of TRNF and is very strong in the reflectance spectrum of the solids. The solution absorption features at 800 and 825 nm were fit using the method of Benesi and Hildebrand (Figure 9b,d).[34] Job plots are also shown to illustrate the preeminence of the 1:1 association ratio (Figure 9c,e). The equilibrium constant is ~90 M^{-1} for D + A ⇌ DA, and the extinction coefficient is 521 and 564 M^{-1} cm^{-1} at 800 and 825 nm, respectively. TRNF is a slightly stronger acceptor compared with DNF but weaker than TENF. The new band at 825 nm is attributed to the donor-to-acceptor charge transfer (DACT) of the complex [Pt(dbbpy)(tdt)][TRNF] in solution. As expected on the basis of its electrochemical potential, TRNF should have less affinity for the electron-rich Pt(dbbpy)(tdt) molecule and be a weaker electron acceptor than TENF. Despite the reduced affinity, a higher extinction coefficient for the TRNF adduct is observed. The near 10-fold increase in magnitude of its extinction coefficient is the primary reason the TRNF adduct asserts a more intense DACT than its TENF counterpart in solution.

The diffuse reflectance data reveal the DACT bands are very strong in the solid state and are readily seen as the dominant absorption bands in the spectra. These bands extend the spectroscopic response far into the NIR region compared with native samples of Pt(dbbpy)(tdt) and the free nitrofluorenones (for which there are no absorptions beyond 450 nm). Such phenomena in the absence of any supramolecular interactions or single electron reduction have been observed with other strong electron acceptors such as $TCNQ^-$.[35]

The absorption data illustrate that DACT bands become more red-shifted with increased acceptor strength. The DACT complex exists in equilibrium with the free components in solution; the concentration of the binary adduct in solution is dependent upon the concentration of the acceptor. Due to solubility limitations for both components and relatively low ε values for the DACT band, it is difficult to observe the band in a 1 cm cuvette. The data for the solid state are dependent upon the stacking mode; data reported here are for samples whose structures were determined prior to collecting their spectra.

The strong D/A interactions and continuous absorptions across the entire visible region and significant portions of the UV and NIR regions for the charge transfer binary systems reported in this work render them remarkable *black absorbers* with a great potential for photovoltaic applications. Supramolecular stack **4**, compared with the sensitizers P3HT or

dx.doi.org/10.1021/ja506583k | J. Am. Chem. Soc. 2014, 136, 16185–16200

CuPc, shows enhanced charge transfer. Its spectral response is red-shifted from those of P3HT and CuPc (Figure 1) without discontinuities. When judged against P3HT, complex **4** accesses the CT state more efficiently through radiative processes (direct absorption); in contrast, P3HT relies on thermal accessibility, which could result in some thermal loss of generated energy.[12a] The spectral behavior of a double-layer CuPc/TCNQ film structure reported by Bortchagovsky et al. showed low energy peaks at 2.85 eV from dissociated TCNQ radicals, which also appeared in the photocurrent spectrum so as to suggest DACT assignment.[12b] However, this DACT band was rather weak, indeed barely discernible within wide-range spectral "gap" area of ca. 2.3−3.2 eV (ca. 375−525 nm); the CuPc/TCNQ binary material exhibits the lowest absorption between the two main donor-dominated major bands at ca. 2.1 and 3.6 eV. Likewise, our previous work on both formally neutral stacks, Pt(dbbpy)(dmid)/TCNQ,[14] and ion-paired stacks, $[Pt(tbtrpy)X]^{+}TCNQ^{-}$ (tbtrpy = 4,4′,4″-$^{t}Bu_3$-2,2′;6′,2″-terpyridine; X = halide or monothiolate),[14b] exhibited relatively minor changes due to DACT vs the spectra of the dissociated donor and acceptor materials. Unlike these CuPc or Pt(II)−diimine−thiolate complexes with TCNQ acceptor species, the binary complexes with nitrofluorenone acceptors herein exhibit remarkably strong DACT absorptions that drastically red-shift the absorption edge with the new absorptions exhibiting similarly strong absorptivity as that of the donor species alone. The effect is most starkly manifest in the new complex **4**, which displays continuous and uniformly strong absorption across the entire UV and visible regions of AM0 and extends into the NIR so as to approach an absorption cutoff of ca. 1300 nm. The band gap is estimated at 0.95, 1.13, and 1.65 eV for **4**, **2**, and Pt(dbbpy)(tdt) solids, respectively. *The continuous absorption profile and extended range are similar to those of silicon and germanium solar cells, which is rather unprecedented in molecular solids.* Although the band gap is more red-shifted for **4**, it is actually beyond the optimal band gap of ca. 1.1 eV needed to attain the Schockley−Queisser theoretical limit of ca. 30% solar cell efficiency for single p−n junction devices.[36] The band gap for **2**, on the other hand, almost matches the optimal Schockley−Queisser band gap.

The spectral behavior outlined for these binary D/A materials are promising for the molecular Pt(diimine)dithiolate donors with the nitrofluorenone acceptors TRNF, TENF, and TCNX that may be pursued as alternatives to divalent metal−phthalocyanine or polythiophene donors with nanocarbon acceptors, most commonly fullerene derivatives, used in the current state-of-the-art OPV devices.[12] The HOMO and LUMO energy levels are also suited for thermodynamically desirable carrier injection and charge separation in Schottky diode and p−n junction OPV device architectures utilizing the donor and acceptor molecules described along with commonly used anode and cathode materials. However, multiple steps and material and device requirements need to be considered (e.g., fabrication of thin films, determining their optical band gaps and absorption coefficients, verification of photocurrent production by photoconductivity measurements, and finally OPV device fabrication and characterization using simulated AM1.5, as opposed to AM0, solar illumination). These will be assessed as we pursue OPV applications of the class of binary systems described here upon suitable chemical structure modifications that would warrant facile fabrication of contiguous thin films via thermal evaporation or solution casting methods. However, this study demonstrates the fundamental characteristics as a backdrop for future OPV studies of this promising class of donor/acceptor materials with a major distinction from previously studied classes of molecular materials in terms of appearance of *strong* DACT absorption bands that are comparable in absorptivity to those of donor species so as to attain a uniformly strong absorption profile across the entire UV and visible AM0 range with considerable penetration into the NIR range. Preliminary studies for the photoconductivity of a thin film of a related Pt complex without an organic acceptor complexed to it are provided at a later section below along with further perspectives on future OPV design possibilities.

NMR Studies. Solutions (5×10^{-4} M) of Pt(dbbpy)(tdt) were prepared in 1 mL of $CDCl_3$, and an equimolar amount of TENF was dissolved in 1 mL of $CDCl_3$ to make a saturated solution. A mixed solution was prepared by weighing the same amounts as the original two NMR samples, then mixing the solids in 1 mL of $CDCl_3$ and placing them in a sonicator bath for 5 min to aid in dissolution. A 0.01 M Pt(dbbpy)tdt solution and an equimolar solution of TRNF were also prepared in $CDCl_3$ then sonicated in the same manner. The equal portions of each solution where then mixed and sonicated. The ^{1}H

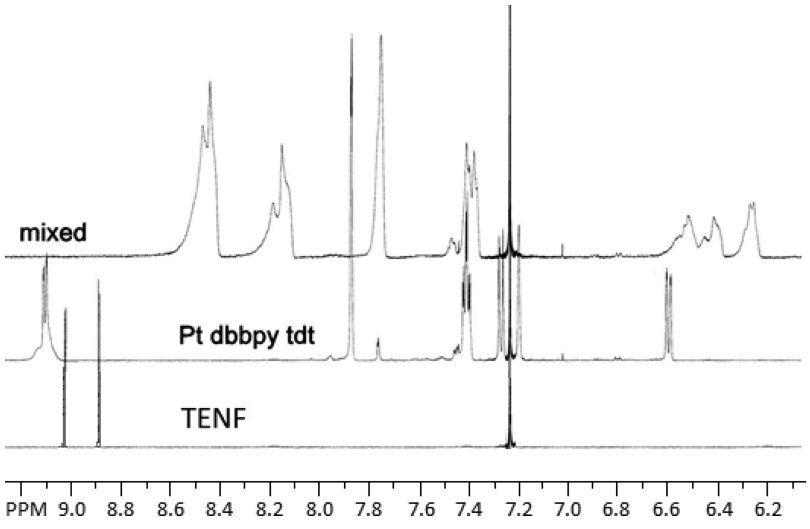

Figure 10. ^{1}H NMR spectra for TENF (acceptor, bottom), Pt(dbbpy)(tdt) (donor, middle), and the mixture of the two in $CDCl_3$ (top).

dx.doi.org/10.1021/ja506583k | J. Am. Chem. Soc. 2014, 136, 16185−16200

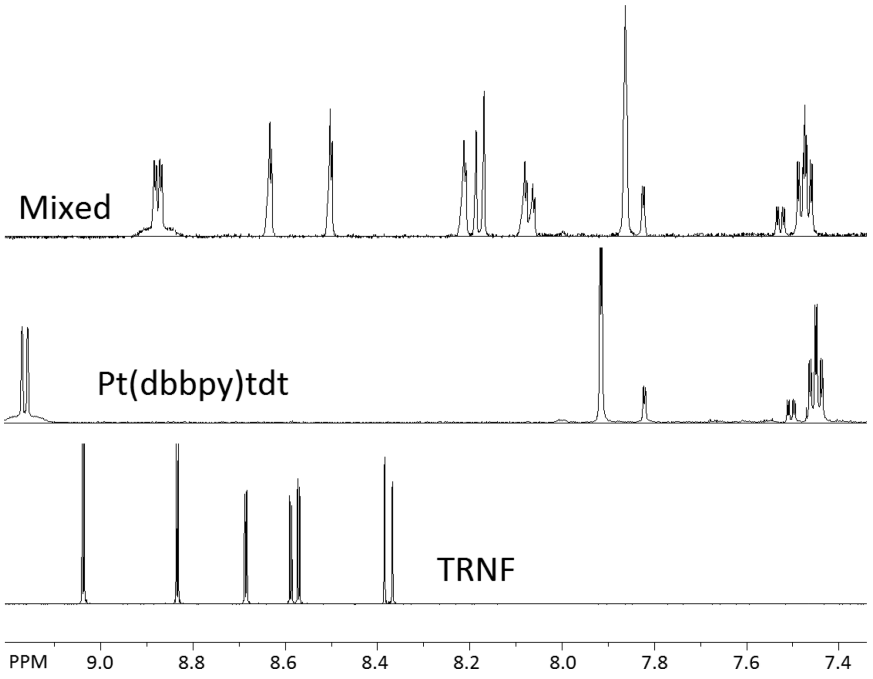

Figure 11. ^{1}H NMR spectra for TRNF (acceptor, bottom), Pt(dbbpy)(tdt) (donor, middle), and the mixture of the two in $CDCl_3$ (top).

NMR spectra for the aromatic region of each sample are depicted in Figures 10 and 11. The aromatic protons should be the most sensitive to small changes in the electronic environment due to intermolecular charge transfer in solution. The data reveal a significant alteration of the electronic environment as all the aromatic peaks are shifted upfield relative to the free components. As well, there seems to be significant peak broadening indicating paramagnetism, which also supports the contention that the DACT process occurs in solution. These data represent rare structural evidence of D/A intermolecular interactions involving closed-shell metal complexes in solution, a situation first reported by Burini et al. for trinuclear d^{10} complexes.[37]

Two-dimensional homonuclear proton NOESY NMR spectra were collected for the Pt(dbbpy)tdt/TRNF solution, presented in Figure 12. These spectra reveal coupling between the aromatic protons of the dithiol moiety of the platinum donor molecule at 7.48 ppm and the aromatic proton at the 3-positon on the nitrofluorenone acceptor at 8.92 ppm (Figure 12). This coupling correlates with the stacking orientation found in the solid crystal state (Figure 3).

Magnetic Susceptibility. Although neither the donor molecule nor any of the nitrofluorenone acceptors contain unpaired electrons that would lead to paramagnetic behavior, **2** exhibits a magnetic moment associated with similar charge transfer complexes.[14a] Magnetic susceptibility measurements (χ_g) where obtained by using the Evans method. Diamagnetic corrections where made for the bipyridine and the magnetic moment by the published method.[38]

The donor−acceptor adduct **2** was determined to have a magnetic moment of $1.07\mu_B$, a notable increase over the donor molecule alone ($0.561\mu_B$). This result is indicative of charge transfer in this binary complex rather than paramagnetism due to formally unpaired electrons.

Solid-State Computational Modeling. Extended Hückel tight binding (EHTB) computational studies were undertaken to probe the structural and spectral properties as they pertain to potential for electrical conductivity applications. The total density of states (DOS) of the D/A stack **4** is shown in Figure 13 along with different projections shown by the shaded areas. From the donor, the more compact platinum d block is located in regions spanning −16.0 and −6.5 eV, while a large sulfur p block containing 80% of the p levels spans between −14.8 and −6.7 eV. For the acceptor N atoms, the major atomic contribution ranges between −16.8 and −8.2 eV, while the O atom contribution is widely dispersed. The computational projections for the solid state packing in **4** reveal a completely occupied band centered at approximately −10 eV with significant contributions from both donor and acceptor atoms (Figure 13). The Fermi level (ε_f) is found to lie in the region of the high DOS at −10 eV and is represented by a horizontal dashed line in Figure 13. These observations suggest that this material should have a metallic behavior in the solid state according to the EHTB level of theory. The strong Pt and S projections below ε_f are consistent with the contention that the Pt−thiolate moiety is the donor part of Pt(dbbpy)(tdt), as well-established for this class of materials (see ref 18, our previous work in ref 14, and references cited therein). On the other hand, contributions from the N and O atoms located on the acceptor moiety in the band structure description of the binary complex lie just above ε_f (see shaded area in Figure 13, right side). This indicates that these atoms of the TENF acceptor have a large contribution to the conduction band of the binary material. The EHTB computation agrees with the electrochemical data, which indicate that the first reduction of the binary adduct is localized on the nitrofluorenone acceptor. These results, taken together with the IR data presented above, support the validity of this model and that charge sharing is occurring in this system. Charge transfer between the donor and acceptor stacks will affect the nitro and carbonyl groups to the greatest degree in the acceptor molecule, as indicated by the computational data and supported by the IR spectra.

The computations suggest also that the close D/A distances are sufficient to allow a stacking overlap with charge

dx.doi.org/10.1021/ja506583k | J. Am. Chem. Soc. 2014, 136, 16185−16200

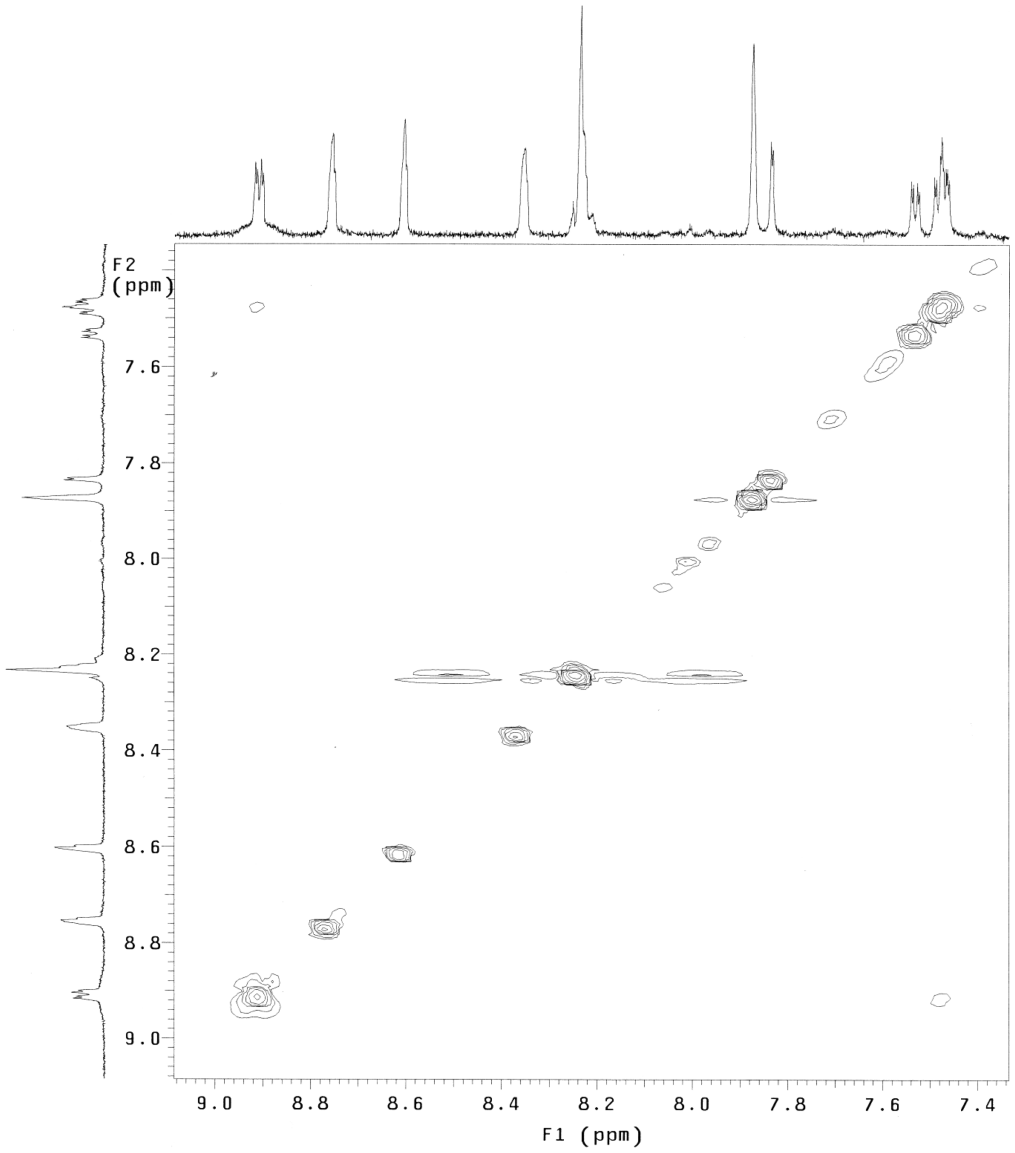

Figure 12. Two-dimensional ^{1}H NOESY NMR spectra for a 0.01 M Pt(dbbpy)tdt/TRNF solution in $CDCl_3$. The 1D spectra parallel to the axis are from the same solution.

delocalization along the linear chains of donor−acceptor species. This type of cooperative solid-state effect is highly desirable for molecular electronics. Systems with significant donor−acceptor intermolecular interactions have been well documented and exploited for many years in materials, such as TTF−TCNQ charge transfer solids.[39] The computational results also suggest the ability to tune the conductivity of binary materials herein by altering the R groups on the ligands in the donor Pt(diimine)-(dithiolate) complex or the number of electron-withdrawing nitro groups on the fluorenone ring of the acceptor molecule.

Preliminary Photoconductivity Studies and Interplay of Structural, Spectral, and Material Properties on Future OPV Designs. In attempts to provide proof-of-concept demonstration of the suitability of the proposed sensitizers for use in OPVs, the Pt(dmecb)(bdt) complex was incorporated into a single layer Schottky diode, and its photoconductivity was evaluated, as shown in Figure 14. The esterified analog of Pt(dbbpy)(tdt) was used in the device analysis for its relative ease of thermal evaporation compared with the alkyl-bearing complex; the dmecb ester group and unsubstituted bdt are moieties that are expected to increase the vapor pressure of the Pt(dmecb)(bdt) complex, hence allowing thin-film fabrication. In contrast, the *t*-Bu and Me substituents in Pt(dbbpy)(tdt) are the likely culprits that precluded the formation of a thermally evaporated thin film even upon rather slow deposition attempts. The solid state spectra in Figure 15 compare the diffuse-reflectance data from which the band gap can be estimated for the two solids. The two Pt complexes Pt(dbbpy)(tdt) and Pt(dmecb)(bdt), therefore, have comparable energy gaps of 1.65 and 1.35 eV, respectively. The photoconductivity data in Figure 14 show a significant photocurrent of ∼0.26 mA at 0.016 V from a 20 nm thin film of Pt(dmecb)(bdt) deposited on a small pixel area (16.2 mm^2), giving rise to a photocurrent density of 1.6 mA/cm^2. Remarkably, this photocurrent value remains essentially constant in the 220−710 nm range that we tested across the UV/vis/NIR region, consistent with the solid diffuse reflectance spectra. This demonstrates that this class of Pt(diimine)-(dithiolate) materials can sensitize a wide range of photon energies within the UV/vis/NIR range of the solar spectrum.

dx.doi.org/10.1021/ja506583k | *J. Am. Chem. Soc.* 2014, 136, 16185−16200

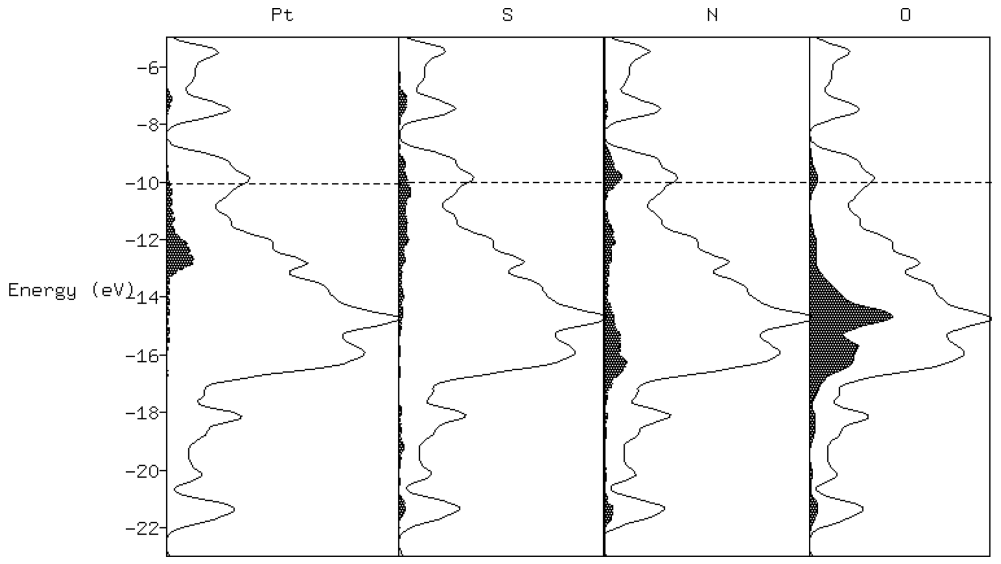

Figure 13. Plot of EHTB density of states of the crystallographic arrangement of complex **4**. Solid curves indicate the total density of state (DOS) (solid line). From left to right, the Pt, S of the donor, and N and O of the acceptor projections are given by the shaded areas that indicate their contributions to the total DOS. The horizontal dashed line corresponds to the Fermi level.

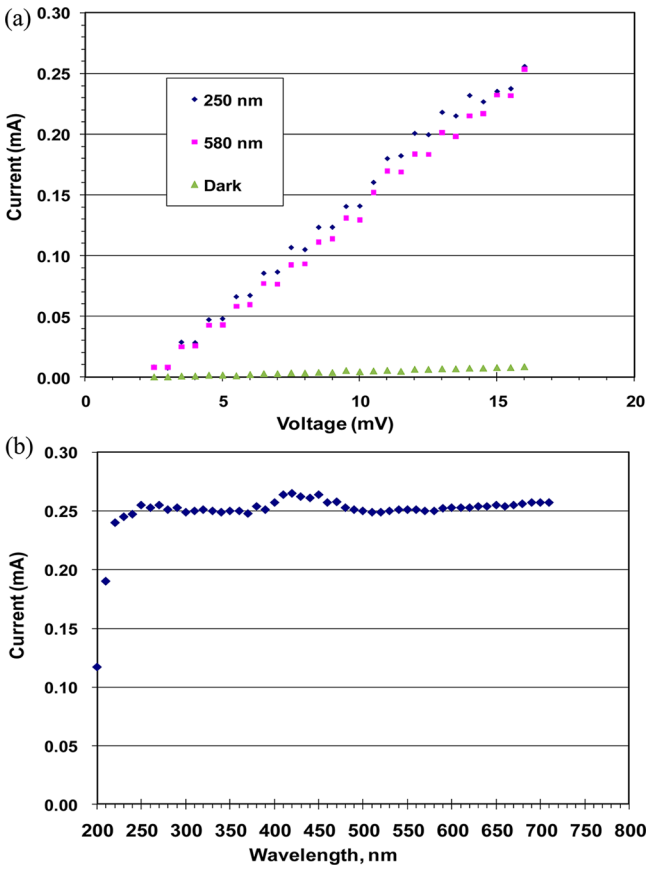

Figure 14. (a) Voltage vs current of a thermally deposited Pt(dmecb)(bdt) Schottky diode under ultraviolet and visible illumination. (b) Current produced by the same diode with ultraviolet and visible illumination.

Unlike the situation for Pt(dbbpy)(tdt), the Pt(dmecb)(bdt) complex does not exhibit red-shifted DACT absorptions with the nitrofluorenone acceptors. Figure 16 shows that, indeed, such adducts exhibit *blue-shifted* absorptions compared with the

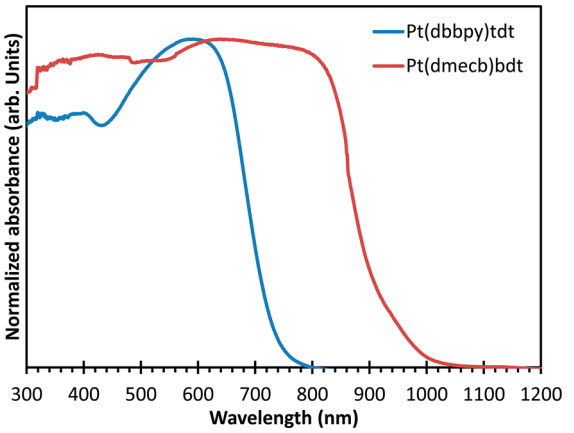

Figure 15. Solid state diffuse reflectance of Pt(dbbpy)tdt and Pt(dmecb)bdt.

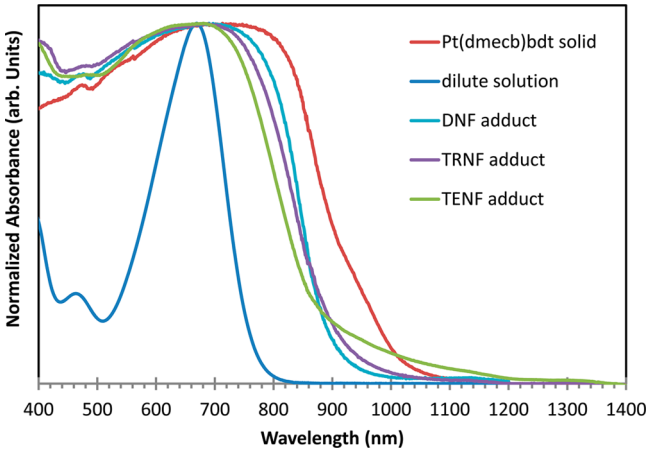

Figure 16. UV/vis spectra of Pt(dmecb)bdt as a dilute CH_2Cl_2 solution, the diffuse reflectance of the pure solid and as adducts with DNF, TRNF, and TENF.

dx.doi.org/10.1021/ja506583k | J. Am. Chem. Soc. 2014, 136, 16185−16200

Pt(dmecb)(bdt) solid! The data, therefore, suggest a competitive circumstance between self-association of the Pt square planar complex on the one hand and DACT adduct formation with the nitrofluorenone acceptor molecule on the other hand. The reduced steric encumbrance in Pt(dmecb)-(bdt) vs Pt(dbbpy)(tdt) favors greater self-association in the former. Additionally, the presence of electron-withdrawing ester groups as bipyridine substituents and the omission of the electron-releasing methyl groups from the dithiolate are factors that render decreased donor potential for Pt(dmecb)(bdt) vs Pt(dbbpy)(tdt), hence inhibiting strong donor−acceptor behavior. Therefore, the overall data in this section demonstrate the interplay of structural (self-association vs donor ability), spectroscopic (red- vs blue-shifted DACT absorptions), and material properties (thermal stability and thin-film formation) for the design of effective OPV devices in the future. Since thermal evaporation was not possible as means to fabricate thin films of Pt(dbbpy)(tdt) and its red-shifted DACT adducts with nitrofluorenones, solution processing will be investigated for such binary adducts and related materials.

■ CONCLUSIONS

Binary donor/acceptor adducts based on Pt(diimine)-(dithiolate) complexes have been prepared, and their potential for solid-state molecular electronic devices has been demonstrated.[18,40] These materials exhibit properties such as close packing that maximizes the intermolecular overlap of the complex units, which act as donors, with molecular units of nitrofluorenone acceptors. Evidence from these studies indicates that the donor/acceptor pairs have a high affinity for one another and engage in cooperative sharing of electron density, contributing to their tendency to form extended linear chains. The class of materials represented by the compounds reported in this paper is an excellent starting point for exploring a new breed of molecule-based solar cells and semiconductors. This potential is demonstrated via the preliminary photoconductivity results for a thin film of the Pt(dmecb)(bdt) complex.

■ ASSOCIATED CONTENT

Supporting Information

X-ray crystallographic files, in CIF format, for complexes **1**−**4** and further electronic spectral data in the solid state and solution. This material is available free of charge via the Internet at http://pubs.acs.org.

■ AUTHOR INFORMATION

Corresponding Authors

omary@unt.edu
dunbar@mail.chem.tamu.edu
shepherd@unt.edu

Author Contributions

‖C.B., J.M.H., and E.W.R. contributed equally.

Notes

The authors declare no competing financial interest.

■ ACKNOWLEDGMENTS

M.A.O. gratefully acknowledges support of this work by the National Science Foundation (Grant CHE-1413641 for supramolecular chemistry aspects; Grant CHE-0911690 for optoelectronic materials design aspects; Grants CMMI-0963509 and CHE-0840518 for infrastructure and instrumentation support, respectively) and the Robert A. Welch Foundation (Grant B-1542 for spectroscopy and bonding aspects). K.R.D. gratefully acknowledges the Welch Foundation (Grant A-1449) and the National Science Foundation (Grant CHE-0957840) for funding of her group's contributions to this work. K.R.D. also acknowledges the National Science Foundation (Grant 9807975) for the funds to purchase the X-ray diffractometer. N.D.S. acknowledges Tao Industries and the National Science Foundation (Grant CMMI-1051502) for supporting his group's contribution to this project within the realm of organic electronics. X.P.W. acknowledges support by the U.S. Department of Energy, Office of Science, under Contract No. DE-AC05-00OR22725 managed by UT Battelle, LLC. The authors also thank Prof. Alan Balch for kindly providing samples of the nitrofluorenone acceptors during earlier stages of this research, Profs. Franky So and Bruce E. Gnade for providing the absorption spectra for thin films of CuPc and P3HT, respectively, and Profs. Michael G. Richmond, Thomas R. Cundari, and W. Justin Youngblood for providing helpful feedback during the Ph.D. defense of C.B. that benefited the finalization of this manuscript.

■ REFERENCES

(1) (a) Ferraris, J.; Cowan, D. O.; Walatka, V. V.; Perlstein, J. H. *J. Am. Chem. Soc.* **1973**, *95*, 948. (b) Coleman, L. B.; Cohen, M. J.; Sandman, D. J.; Yamagishi, F. G.; Garito, A. F.; Heeger, A. J. *J. Solid State Commun.* **1973**, *12*, 1125. (c) Wudl, F. *Acc. Chem. Res.* **1984**, *17*, 227. (d) Williams, J. M.; Ferraro, J. R.; Thorn, R. J.; Carlson, K. D.; Geiser, U.; Wang, H. H.; Kini, A. M.; Whangbo, M.-H. *Organic Superconductors (including Fullerenes)*; Prentice Hall: Englewood Cliffs, NJ, 1992. (e) McConnell, H. M.; Hoffman, B. M.; Metzger, R. M. *Proc. Natl. Acad. Sci. U.S.A.* **1965**, *53*, 46. (f) Long, R. E.; Sparks, R. A.; Trueblood, K. N. *Acta Crystallogr.* **1965**, *18*, 932. (g) Jonkman, H. T.; Kommandeur, J. *Chem. Phys. Lett.* **1972**, *15*, 1972. (h) Konno, M.; Saito, Y. *Acta Crystallogr.* **1974**, *B30*, 1294. (i) Konno, M.; Saito, Y. *Acta Crystallogr.* **1975**, *B31*, 2007. (j) Konno, M.; Ishii, T.; Saito, Y. *Acta Crystallogr.* **1977**, *B33*, 763. (k) Shaik, S. S. *J. Am. Chem. Soc.* **1982**, *104*, 5328. (l) Miller, J. S.; Epstein, A. J. *J. Am. Chem. Soc.* **1987**, *109*, 3850. (m) Miller, J. S.; Zhang, J. H.; Reiff, W. M.; Dixon, D. A.; Preston, L. D.; Reis, E.; Gebert, A. H.; Extine, M.; Troup, J.; Epstein, A. J.; Ward, M. D. *J. Phys. Chem.* **1987**, *91*, 4344. (n) Andruniow, T.; Pawlikowski, M.; Sterzel, M. *Vibr. Spectros.* **1999**, *21*, 45. (o) Milian, B.; Pou-Amerigo, R.; Viruela, R.; Orti, E. *J. Mol. Struct. THEOCHEM* **2004**, *709*, 97.

(2) (a) Bousseau, M.; Valade, L.; Legros, J.-P.; Cassoux, P.; Garbauskas, M.; Interrante, L. V. *J. Am. Chem. Soc.* **1986**, *108*, 1908. (b) Brossard, L.; Ribault, M.; Valade, L.; Cassoux, P. *Phys. Rev. B* **1990**, *42*, 3935. (c) Cassoux, P.; Valade, L.; Kobayashi, H.; Kobayashi, A.; Clark, R. A.; Underhill, A. E. *Coord. Chem. Rev.* **1991**, *110*, 115. (d) Cassoux, P. *Coord. Chem. Rev.* **1999**, *185*−*186*, 213. (e) Kisch, H.; Eisen, B.; Dinnebier, R.; Shankland, K.; David, W. I. F.; Knoch, F. *Chem.—Eur. J.* **2001**, *7*, 738. (f) Alonso, C.; Ballester, L.; Gutiérrez, A.; Perpinan, M. F.; Sanchez, M. A. E.; Azcondo, M. T. *Eur. J. Inorg. Chem.* **2005**, 486.

(3) Alvarez, S.; Vicente, R.; Hoffman, R. *J. Am. Chem. Soc.* **1985**, *107*, 6253.

(4) (a) Shaik, S. S. *J. Am. Chem. Soc.* **1982**, *104*, 5328. (b) McConnell, H. M.; Hoffman, B. M.; Metzger, R. M. *Proc. Natl. Acad. Sci. U.S.A.* **1965**, *53*, 46.

(5) Miller, J. S.; Epstein, A. J. *J. Am. Chem. Soc.* **1987**, *109*, 3850.

(6) (a) Cassoux, P.; Valade, L. In *Inorganic Materials*, 2nd ed.; Bruce, D. W., O'Hare, D., Eds.; John Wiley & Sons: Chichester, U.K., 1996. (b) Tanaka, H.; Okano, Y.; Kobayashi, H.; Suzuki, W.; Kobayashi, A. *Science* **2001**, *291*, 285. (c) Bigoli, F.; Deplano, P.; Mercuri, M.; Pellinghelli, M. A.; Pilia, L.; Pintus, G.; Serpe, A.; Trogu, E. F. *Inorg. Chem.* **2002**, *41*, 5241. (d) Kisch, H. *Comments Inorg. Chem.* **1994**, *16*,

113. (e) Halwa, H. S., Ed. *Handbook of Organic Conductive Molecules and Polymers*; Wiley: Chichester, U.K., 1997; Vol. *1*, pp 200−310.
(7) (a) Coomber, A. T.; Beljonne, D.; Friend, R. H.; Brédas, J. K.; Charlton, A.; Robertson, N.; Underhill, A. E.; Kurmoo, M.; Day, P. *Nature* **1996**, *380*, 144. (b) Robertson, N.; Cronin, L. *Coord. Chem. Rev.* **2002**, *227*, 93.
(8) (a) Geary, A. E. M.; Hirata, N.; Clifford, J.; Durrant, J. R.; Parsons, S.; Dawson, A.; Yellowlees, L. J.; Robertson, N. *Dalton Trans.* **2003**, 3757. (b) Geary, E. A. M.; Yellowlees, L. J.; Jack, L. A.; Oswald, I. D. H.; Parsons, S.; Hirata, N.; Durrant, J. R.; Robertson, N. *Inorg. Chem.* **2005**, *44*, 242. (c) O'Regan, B.; Grätzel, M. *Nature* **1991**, *353*, 737. (d) For a review on Ru based dyes, see: Kalyanasundaram, K.; Grätzel, M. Efficient Photovoltaic Solar Cells Based on Dye Sensitization of Nanocrystalline Oxide Films. In *Optoelectronic Properties of Inorganic Compounds*; Roundhill, D. M., Fackler, J. P., Jr., Plenum Press: New York, 1999; Chapter 5.
(9) (a) Islam, A.; Sugihara, H.; Hara, K.; Katoh, R.; Yanagida, M.; Takahashi, Y.; Murata, S.; Arakawa, H. *New J. Chem.* **2000**, *24*, 343. (b) Islam, A.; Sugihara, H.; Hara, K.; Singh, L. P.; Katoh, R.; Yanagida, M.; Takahashi, Y.; Murata, S.; Arakawa, H. *Inorg. Chem.* **2001**, *40*, 5371.
(10) (a) Yella, A.; Lee, H.-W.; Tsao, H. N.; Yi, C.; Chandiran, A. K.; Nazeeruddin, M. K.; Diau, E. W-G.; Yeh, C.-Y.; Zakeeruddin, S. M.; Gratzel, M. *Science* **2011**, *334*, 629. (b) Nazeeruddin, M. K.; De Angelis, F.; Fantacci, S.; Selloni, A.; Viscardi, G.; Liska, P.; Ito, S.; Takeru, B.; Gratzel, M. *J. Am. Chem. Soc.* **2005**, *127*, 16835. (c) Liyuan, H.; Ashraful, I.; Han, C.; Chandrasekharam, M.; Barreddi, C.; Shufang, Z.; Xudong, Y.; Masatoshi, Y. *Energy Environ. Sci.* **2012**, *5*, 6057.
(11) (a) Rand, B. P.; Xue, J.; Uchida, S.; Forrest, S. R. *J. Appl. Phys.* **2005**, *98*, No. 124902. (b) Xue, J.; Rand, B. P.; Uchida, S.; Forrest, S. R. *J. Appl. Phys.* **2005**, *98*, No. 124903. (c) Shirota, Y.; Kageyama, H. *Chem. Rev.* **2007**, *107*, 953. (d) Coropceanu, V.; Cornil, J.; da Silva Filho, D. A.; Olivier, Y.; Silbey, R.; Brédas, J. *Chem. Rev.* **2007**, *107*, 926. (e) Walzer, K.; Maenning, B.; Pfeiffer, M.; Leo, K. *Chem. Rev.* **2007**, *107*, 1233. (f) Thompson, B. C.; Frechet, J. M. J. *Angew. Chem., Int. Ed.* **2008**, *47*, 58. (g) Peumans, P.; Yakimov, A.; Forrest, S. R. *J. Appl. Phys.* **2003**, *93*, 3693. (h) Al-Amar, M.; Hamam, K. J.; Mezei, G.; Guda, R.; Hamdan, N. M.; Burns, C. A. *Sol. Energy Mater. Sol. Cells* **2013**, *109*, 270.
(12) (a) Bakulin, A. A.; Rao, A.; Pavelyev, V. G.; van Loosdrecht, P. H. M.; Pshenichnikov, M. S.; Niedzialek, D.; Cornil, J.; Beljonne, A.; Freind, R. H. *Science* **2012**, *335*, 1340. (b) Bortchagovsky, E. G.; Kazantseva, Z. I.; Koshets, I. A.; Nešpůrek, S.; Jastrabik, L. *Thin Solid Films* **2004**, *460*, 269.
(13) (a) Zhou, J.; Zuo, Y.; Wan, X.; Long, G.; Zhang, Q.; Ni, W.; Liu, Y.; Li, Z.; He, G.; Li, C.; Kan, B.; Li, M.; Chen, Y. *J. Am. Chem. Soc.* **2013**, *135*, 8484. (b) He, Z.; Zhong, C.; Su, S.; Xu, M.; Wu, H.; Cao, Y. *Nat. Photonics* **2012**, *6*, 593. (c) Kyaw, A. K. K.; Wang, D. H.; Gupta, V.; Zhang, J.; Chand, S.; Bazan, G. C.; Heeger, A. J. *Adv. Mater.* **2013**, *25*, 2397. (d) Zhou, J.; Wan, X.; Liu, Y.; Zuo, Y.; Li, Z.; He, G.; Long, G.; Ni, W.; Li, C.; Su, X.; Chen, Y. *J. Am. Chem. Soc.* **2012**, *134*, 16345. (e) Kyaw, A. K. K.; Wang, D. H.; Gupta, V.; Leong, W. L.; Ke, L.; Bazan, G. C.; Heeger, A. J. *ACS Nano* **2013**, *7*, 4569.
(14) (a) Smucker, B. W.; Hudson, J. M.; Omary, M. A.; Dunbar, K. R. *Inorg. Chem.* **2003**, *42*, 4714. (b) Chen, W.-H.; Reinheimer, E. W.; Dunbar, K. R.; Omary, M. A. *Inorg. Chem.* **2006**, *45*, 2770.
(15) Woolfolk, E. O.; Orchin, M. *Org. Synth., Coll.* **1955**, *3*, 837; **1948**, *28*, 91.
(16) Hodges, K. D.; Rund, J. V. *Inorg. Chem.* **1975**, *14*, 525.
(17) (a) Pucci, D.; Barberio, G.; Crispini, A.; Ghedini, M. *Mol. Cryst. Liq. Cryst.* **2003**, *395*, 155. (b) Case, F. *J. Am. Chem. Soc.* **1946**, *48*, 2574.
(18) Cummings, S. D.; Eisenberg, R. *J. Am. Chem. Soc.* **1996**, *118*, 1949.
(19) *SAINT, Program for area detector absorption correction*; Siemens Analytical X-ray Instruments Inc.: Madison, WI, 1994−1996.
(20) Sheldrick, G. M. *SADABS, Program for Siemens area detector absorption correc-tion*; University of Gottingen: Gottingen, Germany, 1996.
(21) Sheldrick, G. M. *SHELXS-97, A Program for Crystal Structure Solution*; University of Gottingen: Gottingen, Germany, 1997.
(22) Sheldrick, G. M. *SHELXTL, An integrated system for solving, refining, and displaying crystal structures from the diffraction data (Revision 5.1)*; University of Gottingen: Gottingen, Germany, 1985.
(23) Barbour, L. J. *J. Supramol. Chem.* **2001**, *1*, 189.
(24) *APEX2, Program for manipulating second-generation APEX diffractometer*, version 2.1-0; Bruker Advanced X-ray Solutions Inc.: Madison, WI, 2006.
(25) Spek, A. L. *PLATON, A Multipurpose Crystallographic Tool*; Utrecht, University: Utrecht, The Netherlands, 2006.
(26) (a) Hoffman, R.; Lipscomb, W. N. *J. Chem. Phys.* **1962**, *36*, 2179. (b) Hoffman, R.; Lipscomb, W. N. *J. Chem. Phys.* **1962**, *36*, 3489. (c) Hoffman, R.; Lipscomb, W. N. *J. Chem. Phys.* **1963**, *37*, 590. (d) Hoffman, R. *J. Chem. Phys.* **1963**, *39*, 1397.
(27) (a) Landrum, G. A.; Glassey, W. V. *YAeHMOP (Yet Another Extended Hückel Molecular Orbital Package)*; Cornell University: Ithaca, NY, 1995, Version 3.0; freely available on the Web at http://sourceforge.net/projects/yaehmop/ (accessed July 3, 2014). (b) Hoffmann, R. *Solids and Surfaces: A Chemist's View of Bonding in Extended Structures*; VCH Publishers, Inc.: New York, 1988.
(28) (a) Ammeter, J. H.; Elian, M.; Summerville, R. H.; Hoffman, R. *J. Am. Chem. Soc.* **1978**, *100*, 3686. (b) Whangbo, M.-H.; Hoffman, R. *J. Am. Chem. Soc.* **1978**, *100*, 6093.
(29) (a) Mori, T. *Chem. Rev.* **2004**, *104*, 4947. (b) Aldoshina, M. Z.; Goldenberg, L. M.; Zhilyaeva, E. I.; Lyubovskaya, R. N.; Takhirov, T. G.; Dyachenko, O. A.; Atov-Myan, L. O.; Lyubovskii, R. B. *Mater. Sci.* **1988**, *14*, 45. (c) Schirber, J. E.; Over-Myer, D. L.; Carlson, K. D.; William, J. M.; Kini, A. M.; Wang, H. H.; Charlier, H. A.; Love, B. J.; Watkins, D. M.; Yaconi, G. A. *Phys. Rev. B* **1991**, *44*, 4666. (d) Kobayashi, A.; Fujiwara, E.; Kobayashi, H. *Chem. Rev.* **2004**, *104*, 5243. (e) Kobayashi, H.; Tomita, H.; Kobayashi, A.; Sakai, F.; Watanabe, T.; Cassoux, P. *J. Am. Chem. Soc.* **1996**, *118*, 368. (f) Tanaka, H.; Kobayashi, A.; Kobayashi, H. *Chem. Lett.* **1999**, 133. (g) Coronado, E.; Falvello, L. R.; Galán-Mascarós, J. R.; Gómez-García, C. J.; Laukhin, V. N.; Pérez-Benítez, A.; Rovira, C.; Veciana, J. *Adv. Mater.* **1997**, *9*, 984. (h) Shibaevam, R. P.; Yagubskii, E. B. *Chem. Rev.* **2004**, *104*, 5347. (i) Heuzé, K.; Fourmigué, M.; Batail, P.; Canadell, E.; Auban-Senzier, P. *Chem.—Eur. J.* **1999**, *5*, 2971. (j) Heuzé, K.; Mézière, C.; Fourmigué, M.; Batail, P.; Coulon, C.; Canadell, E.; Auban-Senzier, P.; Jérome, D. *Chem. Mater.* **2000**, *12*, 1898. (k) Devic, T.; Evain, M.; Moëlo, Y.; Canadell, E.; Auban-Senzier, P.; Fourmigué, M.; Batail, P. *J. Am. Chem. Soc.* **2003**, *125*, 3295. (l) Kurmoo, M.; Graham, A. W.; Day, P.; Coles, S. J.; Hursthouse, M. B.; Caulfield, J. M.; Singleton, J.; Ducasse, L.; Guinnoeau, P. *J. Am. Chem. Soc.* **1995**, *117*, 12209. (m) Coronado, E.; Galán-Mascarós, J. R.; Gómez-García, C. J.; Laukhin, V. *Nature* **2000**, *408*, 447. (n) Heuzé, K.; Fourmigué, M.; Batail, P.; Coulon, C.; Clérac, R.; Canadell, E.; Auban-Senzier, P.; Ravy, S.; Jérome, D. *Adv. Mater.* **2003**, *15*, 1251. (o) Fourmigué, M.; Reinheimer, E. W.; Dunbar, K. R.; Auban-Senzier, P.; Pasquier, C.; Coulon, C. *Dalton Trans.* **2008**, 4652.
(30) Olmstead, M. M.; Jiang, F.; Attar, S.; Balch, A. L. *J. Am. Chem. Soc.* **2001**, *123*, 3260.
(31) Rawashdeh-Omary, M. A.; Omary, M. A.; Fackler, J. P., Jr. *J. Am. Chem. Soc.* **2001**, *123*, 9689.
(32) Kuder, J. E.; Pochan, J. M.; Turner, S. R.; Hinman, D. F. J. *Electrochem. Soc.* **1978**, *125*, 1750.
(33) Chappell, J. S.; Bloch, A. N.; Bryden, W. A.; Maxfield, M.; Poehler, T. O.; Cowan, D. O. *J. Am. Chem. Soc.* **1981**, *103*, 2442.
(34) Benesi, H. A.; Hildebrand, J. H. *J. Am. Chem. Soc.* **1949**, *71*, 2703.
(35) Jonkman, H. T.; Kommandeur, J. *Chem. Phys. Lett.* **1972**, *15*, 496.
(36) Shockley, W.; Queisser, H. J. *J. Appl. Phys.* **1961**, *32*, 510.
(37) Burini, A.; Fackler, J. P., Jr.; Galassi, R.; Macchioni, A.; Omary, M. A.; Rawash-deh-Omary, M. A.; Pietroni, B. R.; Sabatini, S.; Zuccaccia, C. *J. Am. Chem. Soc.* **2002**, *124*, 4570.
(38) (a) Johnson, B. F. G.; Benfield, R. W. *Topics in Inorganic and Organometallic Stereochemistry*; Geoffroy, G. L., Ed.; Wiley: New York,

1981. (b) Figgis, B. N. Ligand Field Theory. In *Comprehensive Coordination Chemistry*; Wilkinson, G., Ed.; Pergamon: Oxford, U.K., 1987; Vol. *1*, Chapter 6, p 213.
(39) Claessen, R.; Sing, M.; Schwingenschlögl, U.; Blaha, P.; Dressel, M.; Jacobsen, C. S. *Phys. Rev. Lett.* **2002**, *88*, No. 096042.
(40) Mayer, A. C.; Kazmirov, A.; Malliaras, G. G. *Phys. Rev. Lett.* **2006**, *97*, No. 105503.